Vat-photopolymerization of ceramic materials: exploring current applications in advanced multidisciplinary fields

frontiers | Frontiers in Materials

TYPE Review
PUBLISHED 09 October 2023
DOI 10.3389/fmats.2023.1242480

OPEN ACCESS

EDITED BY
Annan Chen,
Huazhong University of Science and Technology, China

REVIEWED BY
Uday M. Basheer Al-Naib,
University of Technology Malaysia, Malaysia
Ye Dong,
Tsinghua University, China

*CORRESPONDENCE
Elisa Fiume,
elisa.fiume@polito.it

RECEIVED 19 June 2023
ACCEPTED 19 September 2023
PUBLISHED 09 October 2023

CITATION
Fiume E, Coppola B, Montanaro L and Palmero P (2023), Vat-photopolymerization of ceramic materials: exploring current applications in advanced multidisciplinary fields. *Front. Mater.* 10:1242480. doi: 10.3389/fmats.2023.1242480

Vat-photopolymerization of ceramic materials: exploring current applications in advanced multidisciplinary fields

Elisa Fiume*, Bartolomeo Coppola, Laura Montanaro and Paola Palmero

INSTM R.U. Lince Laboratory, Department of Applied Science and Technology (DISAT), Politecnico di Torino, Torino, Italy

Additive manufacturing has brought about a real revolution in the manufacture of objects in a variety of application areas, overturning the traditional paradigm based on subtractive approaches. The potential benefits deriving from the application of these techniques in the field of ceramic materials extend to different industrial sectors, leading to shorter, more accurate and cost-effective manufacturing processes. Within the present review, we provide a transversal analysis of the state-of-the-art of the applications of vat-photopolymerization technologies, namely, stereolithography and digital light processing in relevant technological industrial/research fields of our times, including biomedicine, energy, environment, space and aerospace, with a special focus on current trends and project-specific requirements. Unmet challenges and future developments will be discussed as well, providing readers a transfer of knowledge and "lessons learned" from one field to the other, being this approach aimed at the further growth of the technology towards its industrialization and market uptake.

KEYWORDS

VAT-photopolymerization, laser stereolithography, digital light processing, advanced ceramics, biomedical, space/aerospace, energy, environment

1 Introduction

Ceramic materials have always played a pivotal role in the development of advanced technological applications, including biomedicine (Chen Y.-W. et al., 2016; Rahmati and Mozafari, 2019; Chandra Babu Naidu and. Suresh Kumar, 2020), energy, environment (Jiang et al., 2010; Singh et al., 2021), space and aerospace (Steyer, 2013; Soboyejo et al., 2015).

Besides traditional ceramics, advanced ceramics have recently captured the interest of the scientific community due to the possibility to produce highly performant ceramic components from highly pure raw materials, meeting specific requirements in advanced industrial and research fields.

Compared to traditional ceramics, advanced ceramics exhibiting a tailored micro- or nano-scale structure are usually characterized by high hardness and strength, excellent performances at high temperatures, low friction coefficient, as well as high chemical stability even in extreme environments.

Table 1 provides a classification of advanced ceramics basing on chemical/physical properties and intended use and application field.

For many years the full potential of ceramic materials has been strongly restrained by inherent limitations existing in traditional ceramic manufacturing processes, such as dry pressing (Bortzmeyer, 1995), tape casting (Jabbari et al., 2016), slip casting (Tiller and Tsai, 1986), gel casting (Pollinger et al., 2016) and injection molding (Edirisinghe and Evans, 1986). Most of these techniques, in fact, do not allow the production of ceramic parts with complex and highly detailed geometries. In addition, the high hardness and brittleness typical of ceramic materials make it difficult to process components after sintering. This operation is often associated to the generation of defects and internal stresses inside the component, which are potentially able to induce its mechanical failure in operation (Tuersley et al., 1994; Rakshit and Das, 2019). Last but not least, molds are usually required in traditional ceramic manufacturing as intermediate tools, resulting in expensive and time-consuming procedures.

Part of these technical limitations have been resolved in the 1980s with the advent of Additive Manufacturing technologies, which completely overturned conventional processing of polymer, metal and ceramic materials applied to different industrial fields (Wohlers and Gornet, 2016). Unlike traditional top-down approaches based on the production of three-dimensional (3D) objects by subtraction of material from a single block, the expression Additive Manufacturing (AM), or Solid Freeform

TABLE 1 Classification of advanced ceramics according to their characteristics and main applications.

Class	Characteristics	Applications examples	Ref
Structural ceramics	Enhanced mechanical properties under demanding conditions	Adiabatic diesel turbine and automotive engines	Schoenung (2001)
		Aerospace systems	
		Heat exchangers	
		Electronic devices	
		Medical devices	
		Cutting tools	
		Metal machining	
		Military devices	
Electro-ceramics	Piezoelectric, ferroelectric or dielectric response	High-capacity dielectric devices	Salame and Kolte (2020)
		Non-volatile memories (DRAMs)	
		Energy storage and conversion	
Opto-ceramics	Transparency Piezoelectric, ferroelectric or dielectric response	Variable optical attenuators	Jiang et al. (2005)
		Polarization controllers	
		Sinusoidal filters	
		Dynamic gain flattening filters	
		Tunable optical filters	
		Q-switches	
Ceramic coatings	Thermal insulation	Thermal barrier coatings (TBC) Environmental barrier coatings (EBC)	Lee, (2000); Cao et al., 2004; Shrirao and Pawar, (2011); Verband der Keramischen Industrie, (2022)
	Electrical insulation		
	Wear/corrosion protection to vulnerable surfaces		
Bioceramics	Biocompatibility	Scaffolds for bone repair and regeneration	Chevalier and Gremillard (2009)
		Dental prostheses	
		Joint replacement	
Superconductors	Superconductivity above 77 K	Advanced electronic packages and devices	Humphreys, (1991); Klauda et al., 2000; Rokhvarger and Chigirinsky, (2004)
		Communication satellites	
		Base transceiver stations	
		Noise reduction filters	
		Input-multiplexer channel filters	

Fabrication (SFF) technologies encompasses a series of advanced manufacturing techniques based on a layer-by-layer approach (bottom-up), where the final object is progressively built by the successive deposition of adjacent layers generated through a slicing procedure from a computer-based 3D model, until the complete geometry is reproduced (Cawley, 1999).

According to the specific method of layer manufacturing and deposition strategy, the American Society for Testing and Materials (ASTM) classifies AM technologies into 7 different categories: i) vat-photopolymerization, ii) material jetting, iii) binder jetting, iv) material extrusion, v) powder bed fusion, vi) sheet lamination and vii) directed energy deposition (ASTM ISO/, 2022).

Regardless of materials nature, vat-photopolymerization processes, namely, Stereolithography (SL) and Digital Light Processing (DLP), definitely stand out for high-quality surface finishing and resolution, as well as relatively quick building times and reproducibility, associated to a very high potential for industrial production.

The invention of SL is attributed to Charles Hull, who first combined Computer-Aided Design (CAD), photo-chemistry and polymer processing for producing three-dimensional plastic objects by irradiating liquid photocurable monomers (Hull, 1988).

The process, patented in 1986, immediately entailed a number of significant advantages, first and foremost the possibility of obtaining highly-complex geometries by simply coupling a SL device and a computer for generating the 3D design of the object and making any changes in the model. In this way, neither additional expensive tools nor recurring operator interventions were required, with a considerable gain in terms of time, resources, and process reliability, resulting in the overall shortening of the design/manufacturing cycle (Hull, 1986).

Traditional SL, originally optimized for photocurable polymers, was adapted to ceramic materials only in 1994 by Griffith and coworkers (Griffith and Halloran, 1994). This event marked the advent of ceramic SL, an innovative ceramic processing technique based on the use of ceramic resins, i.e., reactive colloidal systems consisting of photocurable liquid monomers, photo initiator, ceramic particles, dispersant and eventual additives such as diluents and solvents.

Generally, the costs associated to an additive manufacturing process are independent on the geometric characteristics of the part and depend solely on the nature of the material selected for the intended purpose and the quantity/size of parts to be produced. Compared to other classes of materials, this specific aspect represents an added value in ceramic processing, often consisting of accurate small batch productions, mostly in the form of customized prototypes (Lakhdar et al., 2021).

The aim of the present review is to provide a comprehensive state-of-the-art of the applications of SL and DLP in relevant technological industrial/research fields of our times, including biomedicine, energy, environment, space and aerospace. Instead of focusing on single application, the highly transversal nature of this paper will emphasise the versatility of the techniques towards the fabrication of components for many different sectors, with the aim of providing potential readers a transfer of knowledge and "lessons learned" from one field to the other, with a win-win approach. Special attention will be paid to the design of porous components, densities and mechanical properties, in relation to contemporary applications of the technology. Current trends, unmet challenges and future developments will be discussed as well.

A schematic diagram showing the structure of the present review is provided in Figure 1.

2 Ceramic vat-photopolymerization: from 3D models to finished ceramic products

Ceramic SL and DLP belong to the family of vat-photopolymerization technologies, based on the interaction of a light source with photosensitive liquid monomers loaded with ceramic particles. The 3D object is built by selectively exposing each bidimensional layer to the radiation at a defined wavelength, inducing the polymerization of the liquid resin into the desired shape.

Within typical SL and DLP processes, 3D object is built in five stages, as depicted in Figure 2.

a) Elaboration of the 3D model
b) Preparation of the ceramic resin
c) Vat-photopolymerization
d) Debinding
e) Sintering

An in-depth discussion of the various steps is presented in the following.

2.1 Elaboration of the 3D model

The first step towards the realization of a new ceramic component by SL and DLP is the elaboration of the 3D model, which defines the geometrical details and features to be reproduced.

As mentioned earlier, one of the major advantages of SL and DLP, compared to traditional shaping processes, lies in the greater freedom of choice of parts geometries and complexity. This is particularly true in the case of art and design applications, where the only existing limits lie in the imagination of the designer.

On the other hand, concerning highly specialized and technical fields as medicine, energy, environment, space and aerospace, the choice of the 3D model is strongly conditioned by the specific applications, defining the performances of the component in operation.

A first macro-distinction in terms of design allows to identify two different types of 3D structures, i.e., bulk and porous components.

Bulk components are characterized by dense volumes shaped either as elementary 3D solids, or characterized by application-specific shapes.

Elementary geometries are typically produced for preliminary microstructural/crystallographic analyses and mechanical testing, where sample geometry and dimension are specified by ASTM standards. Common mechanical tests for the characterization of bulk technical ceramics include flexural strength (beams with rectangular cross section), biaxial flexural strength (thin discs) and fracture toughness (notched beams). For further information

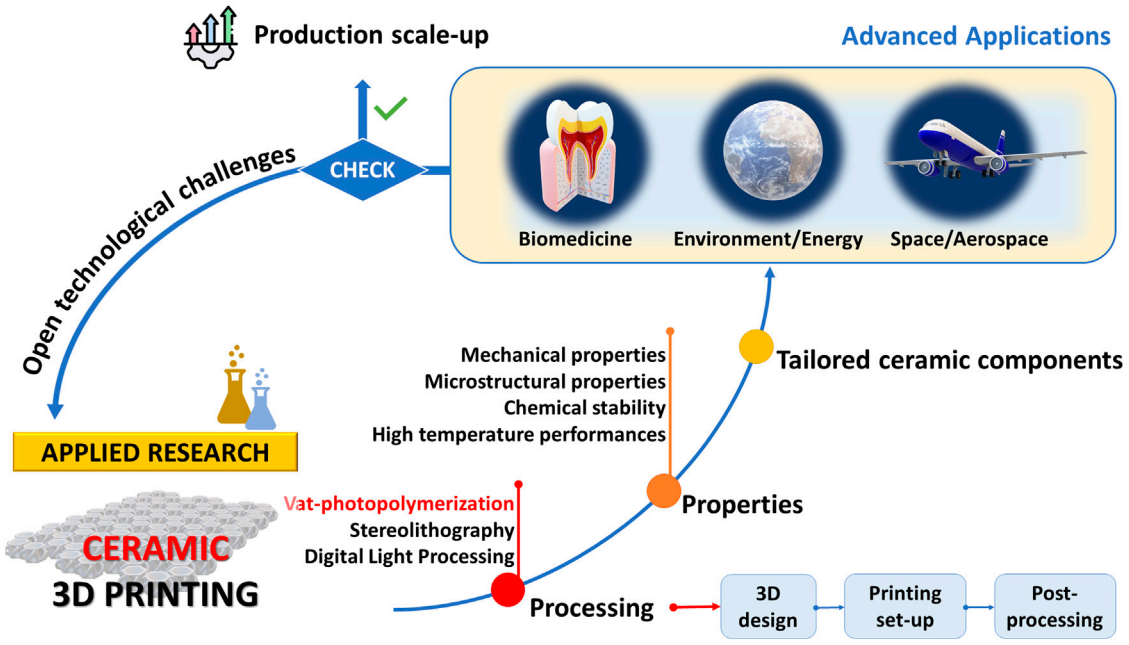

FIGURE 1
Schematic diagram of the review structure.

on nominal geometrical dimensions, equipment and testing protocols, readers could refer to (ASTM C1499-19, 2019; ASTM C1161, 2023; ASTM C1421, 2023).

Concerning application-specific 3D components, endo-osseous implants, crowns and bridges for dental applications (Dehurtevent et al., 2017; Lian et al., 2018; Li et al., 2019; Li et al., 2020c), ceramic cores for hollow aeroengine turbine blades and ceramic casting molds (Zhou et al., 2010; An et al., 2022) are certainly among the most representative examples of bulk components. Additional details on design and requirements will be provided in the following.

Within a structured and systematic research activity, the manufacturing of bulk components is often preparatory to the realization of cellular ceramics and may hold even greater technological challenges. In structural applications, in fact, an accurate knowledge of the intrinsic mechanical properties of the constituent material in relation to post-processing conditions, shape and size of the component, may be crucial for predictive purposes (D'Andrea et al., 2023).

A wide variety of 3D porous architecture is described in literature (Figure 3), from architectures derived from lattice structure design methods (Figure 3 a-b) (Pan et al., 2020) to nature-inspired structures (bone-inspired trabecular-like structures (Liu et al., 2021c) honeycomb structures (Zakeri et al., 2021) and gyroids from butterfly wings (Gan et al., 2016)) (Figures 3C–1, c-2 and c-3).

Strut-based lattices are characterized by the periodical repetition in the 3D space of a unit cell characterized by different geometries (Figure 3A). Properties gradient can be introduced by several strategies in order to meet specific physical or mechanical requirements, either by varying the number of unit cells or combining different unit cells within a single 3D model (Seharing et al., 2020; Zhao et al., 2020).

Common applications of porous ceramics include lightweight infill, grafts for tissue engineering applications and energy absorber or micro-reactors (Feng et al., 2018), where the selection of the 3D porous structures depends on specific application requirements.

Concerning biomedical field, the design of bioinspired 3D architectures (scaffolds) resembling natural bone has long been corroborated all over the world, allowing to optimise the cellular response and performance of the device after implantation.

Stochastic architectures, including foam-like and trabecular-like structures for bone tissue engineering applications, are usually obtained by Voronoi tessellation method (Liu et al., 2021c), which generates virtual isotropic 3D structures perfectly matching the main histo-morphometric indices characterizing trabecular bone, thus conferring a certain degree of biomimicry to the implantable device. In these cases, particular attention should be paid to pore size and interconnection, as well as structural properties of the scaffold, with the aim of optimizing mass transport properties, cell migration and vascularization of the graft after implantation while guaranteeing mechanical support.

Besides bone regeneration, the use of stochastic foam-like structures has also attracted considerable interest in the development of modern catalytic supports. In fact, their tortuous internal pore structure is capable of generating turbulent flows, resulting in enhanced chemical activity compared to traditional honeycomb structures (Dimopoulos Eggenschwiler et al., 2009).

Recently, special attention was addressed to triply periodic minimal surface (TPMS) porous structures (Figure 3B), which are generated mathematically to have a zero-mean curvature at each point; at the same time evidence of TPMS structures in natural materials and in the animal world (Al-Ketan and Abu Al-Rub, 2019; Ahamed et al., 2022) can be found as well.

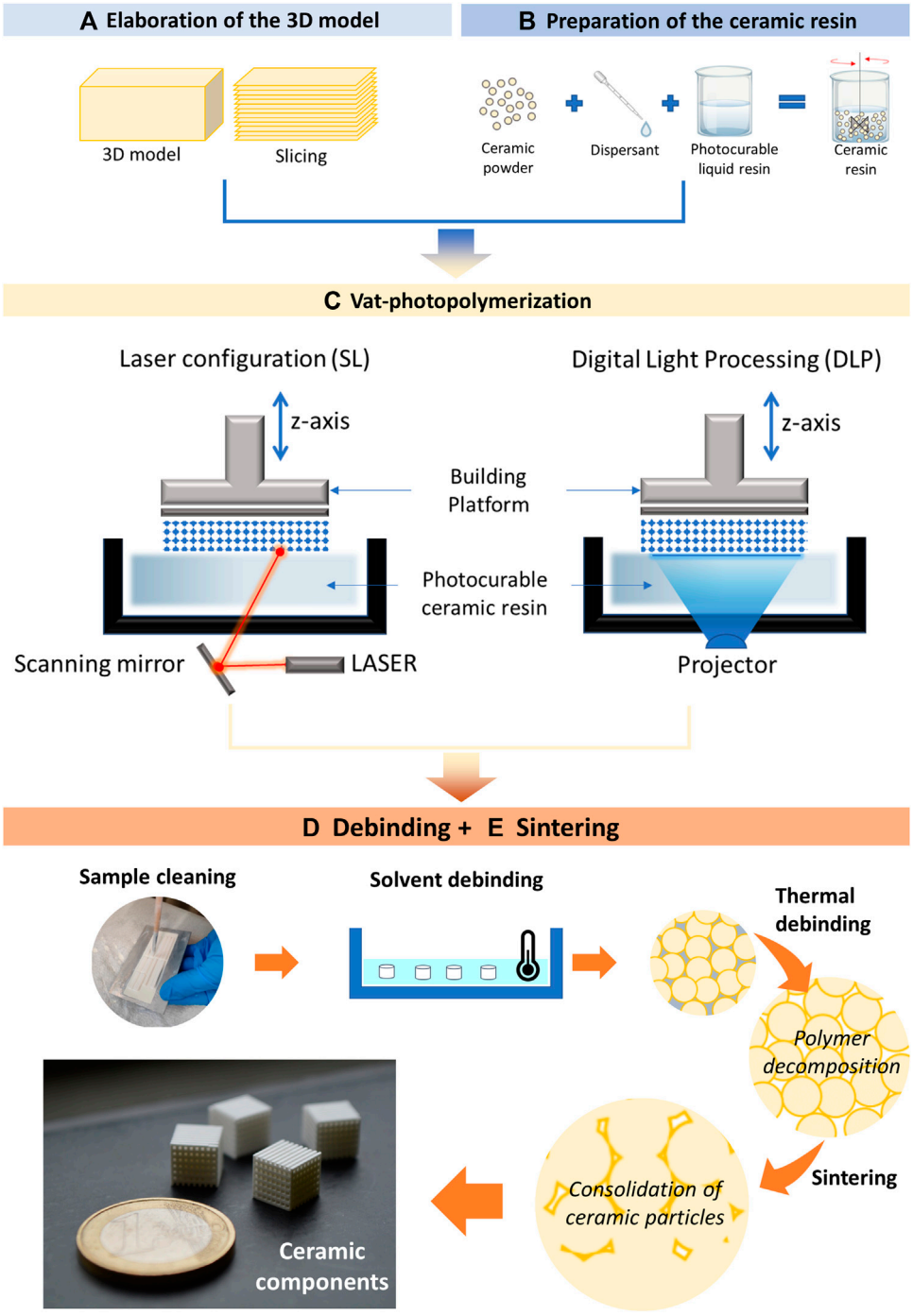

FIGURE 2
Operational steps of typical SL and DLP processes: **(A)** Elaboration of the 3D model; **(B)** Preparation of the ceramic resin; **(C)** Vat-photopolymerization; **(D)** Debinding and **(E)** Sintering.

TPMS architectures show a great potential both in medical and environmental/energy field due to a profitable combination of properties, including specific and axisymmetric stiffness, high surface-to-volume ratio and interconnected porous structure (Maskery et al., 2018). Owing to these properties, TPMS lattices find applications both as scaffolding structures for bone regeneration (Dong and Zhao, 2021) and architected catalytic ceramic substrates to control internal combustion engines emissions and gas processing in the downstream operations of gas and oil industry (Al-Ketan et al., 2019). In TPMS structures, in fact, the high surface-to-volume ratio favors the diffusion of the catalyst preventing its trapping in the corners due to the presence of smooth surfaces.

Finally, it is worthy to be mentioned, the tailoring of complex parts modeling depending on fluid transport properties. Indeed,

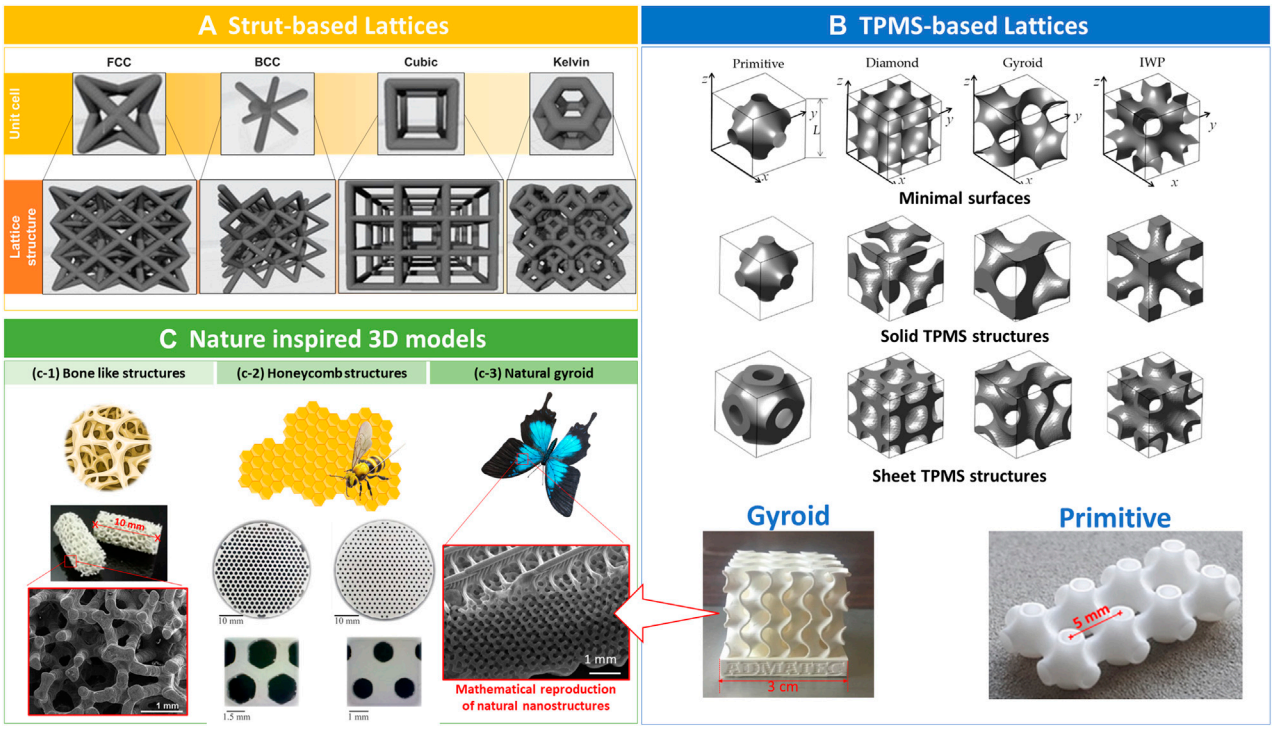

FIGURE 3
Examples of porous 3D structures: **(A)** Unit cells for strut-base lattices (Lu et al., 2022); **(B)** TPMS-based lattices (Yeranee and Rao, 2022) and digital photographs of gyroid and primitive ceramic components (Courtesy of Lince Laboratory (DISAT), Politecnico di Torino); **(C)** Nature inspired 3D models including (c-1) trabecular-like scaffolds (Baino et al., 2022) honeycomb "stack" structure (c-2) (Spirrett et al., 2022) and (c-3) natural gyroid (Pelanconi and Ortona, 2019). Images **(A)**, **(B)** (c-3) adapted and (c-2) reproduced under the Creative Commons Attributions CC BY license. Image (c-1) adapted under the Creative Commons Attribution 4.0 International Public license.

permeability, pressure drop and fluid flow-induced wall shear stress are important properties to be considered for porous parts to be used in numerous fields, namely, biomedical, environmental, energy, space and aerospace. To this extent, computational fluid dynamics (CFD) is a useful tool to optimize the structure of the object to be printed, such as scaffolds (Ali et al., 2020; Lei et al., 2022; Prakoso et al., 2023), membranes/filters (Kovacev et al., 2021; Chevarin et al., 2023), nozzles (Naveen Kumar et al., 2017). In the case of bone tissue engineering, in which bioactivity, cell differentiation and proliferation within the scaffolds are fundamental, numerous parameters of the scaffold can be varied and tested thanks to CFD avoiding expensive and time-consuming experimental trials. For example, considering the permeability of different human bones (vertebral body 0.359×10^{-8} m^2; vertebral body lumbar 1.09×10^{-8} m^2; tibia 0.768×10^{-8} m^2), that is strictly related to the transportation of nutrition and oxygen for cells proliferation and growth, scaffolds can properly be modeled and validated trough CFD according to their final application (Lei et al., 2022). Also in the environmental field, for example, in the case of exhaust gas purification with ceramic substrates coated with catalytic converter, CFD can aid the design of the new catalytic supports. Indeed, traditional supports are made by extrusion processes while 3D printing open the way to new and complex structures. The possibility to print complex designs having higher porosity (e.g., lattice structures in contrast to traditional honeycomb) results in lower pressure drop across the support (Kovacev et al., 2021).

After the generation of the 3D model, a slicing procedure is required to generate overlapping layers composing the final object. Just as the number and size of pixels determine the quality and the sharpness of an image, the resolution of a ceramic component produced by SL and DLP technologies is strongly dependent on the slicing procedure and in particular on the thickness of each layer. However, if for elementary geometries, such as cubes or discs, the layer thickness has little influence on shape definition and resolution, in the case of more complex and irregular geometries, thick layers could produce an unpleasant "step effect" on the printed object surface, resulting in the introduction of a certain surface roughness as well as a significant geometric deviation from the original 3D model.

Thus, layer thickness has to be set within a proper range, usually between 15 μm and 100 μm, where lower limits are usually dictated by the SL apparatus, while upper limits depend on the compromise between surface resolution requirements and curing depth, as discussed in the next paragraph.

2.2 Preparation of the ceramic resin

Ceramic feedstock for vat-photopolymerization processing include both photocurable ceramic resins and preceramic resins.

Ceramic resins, or photocurable suspensions, consist of pure photocurable resins modified by the addition ceramic fillers,

heterogeneously dispersed within the liquid media. This brings additional challenges compared to traditional SL polymer processing as it is responsible for major changes in slurry quality and response upon UV exposure.

In fact, it has been shown that the addition of a ceramic filler within the monomer can significantly alter both the rheology of the slurry and its interaction with the light source, with consequences on the printing outcome (green bodies) and the properties of the sintered parts.

When designing the composition of a photocurable ceramic resin for SL and DLP, slurry viscosity, shear thinning behavior, dispersion stability, curing properties and surface quality of the green bodies are of primary importance.

In general, three main factors must be taken into consideration for the development of an optimal photocurable ceramic slurry.

- The concentration (solid loading) and the size of the ceramic particles, which are responsible for light scattering phenomena and rheological changes;
- The optical properties of the ceramic particles, such as the refractive index and UV-light absorption;
- The presence of additives, such as dispersing and absorbing agents to tune slurry rheological and optical properties.

Light scattering can be described as the change in light direction occurring in the presence of non-uniformities within the medium, represented by ceramic particles. Light scattering within ceramic resins depends on several factors including median particle size, particles concentration and the refractive index mismatch (ΔRI) between ceramic particles and resin.

In order to optimize light-resin interactions, minimum criteria to be followed for the selection of the ceramic solid load are (Zakeri et al., 2020).

1. Minimum ΔRI, where the RI for ceramics usually ranges between 1.56 and 2.6, while most of the vat-polymerization resins are characterized by a RI of about 1.5.
2. Median particle size of ceramic particles should be lower than the layer thickness (0.05 μm < D50<10 μm), to improve resolution along the *z*-axis, perpendicular to the building platform.

In general, a high solid loading is required to obtain high green density values and minimize shrinkage upon drying and sintering, thus allowing to achieve high fired densities in the sintered parts (Zakeri et al., 2020). In these regards, Inserra and coworkers (Inserra et al., 2023) reported an increase in fired density of Ce-ZrO_2/Al_2O_3 composites, from 94%TD to 97%TD, by increasing the solid loading from 50 to 60 wt%. Analogously, increasing trends of the green density were observed as function of the solid loading, both in the presence and in the absence of dispersing agents. At the same time, the effect on the curing behavior was investigated, observing a decrease of the curing depth as particles concentration increased (Inserra et al., 2023).

In fact, the higher the concentration of particles, the greater the light scattering phenomena, as each ceramic particle acts as scattering centre of the incident light (Wu et al., 2005). As a consequence of the decrease in curing depth, an increase of the curing width can be observed, determining lower printing accuracy and higher weakness of interlayer bonding, respectively (Gentry and Halloran, 2013; Pan and Chen, 2016).

In order to control light scattering phenomena, some studies reported the use of light absorbing agents (dye) to absorb photons and control the overgrowth, thus improving the printing precision (Ye et al., 2021; Chen et al., 2022c). However, as the dye and the photoinitiator compete to absorb light, lower energy is absorbed by the photoinitiator, decreasing the photopolymerization reaction. As a consequence, the amount of dye has to be properly selected in order to preserve minimum curing depth requirements, as explained in Paragraph 2.3.

Concerning rheological properties, low-viscosity photocurable resins (below 5,000 mPa s (Hinczewski et al., 1998)) are required to facilitate an even material distribution upon feeding and surface recoating. Shear viscosity values have to be optimized on the basis of the operating share rate, usually between 100–200 s^{-1}. To improve the quality of photocurable ceramic resins, dispersants can be added to the resin formulation to keep ceramic particles dispersed and stabilize the slurries (Kim et al., 2022; Inserra et al., 2023). The dispersant concentration is usually optimized as function of the solid loading, allowing to achieve higher particles concentration as well as desirable flowability, curing behaviour and surface quality of green samples. In fact, under optimal conditions, dispersant molecules form a kind of protective layer around the ceramic particle surface, providing a repulsive effect and suppressing the attraction of particles to each other. In this way, agglomeration and flocculation phenomena can be efficiently managed, thus ensuring low slurry viscosity and good dispersibility (Kim et al., 2022).

Besides ceramic resins, the use of pre-ceramic polymers represents a valuable alternative to the processing of high viscous suspensions or coloured ceramics affected by high absorption in the UV range. Preceramic polymers consist of a homogeneous mixture of resins containing ceramic precursors to obtain polymer derived ceramics upon thermolytic decomposition. This strategy has been successfully implemented for obtaining Si-based bicomponent and multicomponent ceramic parts. More specifically, polycarbosilanes, polysiloxanes, polycarbosilazane and polyborosilazane have been proposed as precursors of SiOC, SiC, SiCN and SiBCN ceramics, respectively (Zanchetta et al., 2016; De Hazan and Penner, 2017; Li et al., 2018; Wang et al., 2019).

2.3 SL and DLP processes

According to the type of light source used to cure the liquid resin, two different vat-photopolymerization configurations can be defined.

(a) Laser configuration (SL), which uses a UV laser to scan the printing area and light-cure the resin dot by dot.
(b) DLP, based on the presence of a digital light projector screen. In this configuration, a Digital Mirror Device (DMD) allows the simultaneous irradiation of the whole layer at once, which makes DLP considerably faster compared to laser-based SL (Chaudhary et al., 2022).

Successful SL and DLP processes are the result of the combination of multiple and closely related factors, and a set of printing parameters have to be optimized as function of ceramic resin and geometries to be printed. The leading triad is certainly

composed of exposure time, energy dose and layer thickness of the slicing model. The proper combination of exposure time and energy dose not only determines the dimensional resolution of the printing process, allowing overcuring problems to be limited, but defines the optimal curing depth for a given photocurable resin. Indeed, two concurring phenomena must be considered: on one hand, the curing depth should be at least 1.5 times the layer thickness, in order to improve the adhesion between adjacent layers and prevent delamination phenomena due to a poor curing; on the other hand, exposure parameters should not exceed optimal values to avoid overcuring resulting in parts low lateral resolution. In some cases (e.g., high solid loadings, ceramic particles optical properties, UV-absorbing materials, *etc.*) curing depth can be efficiently increased both by increasing energy dose and exposure time. Another strategy to increase curing depth relies on the increase in photoinitiator concentration within the resin formulation, determining an increase in monomer-to-polymer conversion. Readers can find additional details on the photopolymerization of ceramic resins for SL and DLP in Refs. (Zakeri et al., 2020; Lakhdar et al., 2021; Bove et al., 2022; Chaudhary et al., 2022).

2.4 Debinding

As soon after printing, residual liquid resin should be accurately removed by different solvents, yielding *green bodies,* consisting of ceramic particles embedded into a rigid polymeric matrix.

Green bodies are then subjected to thermal debinding, which allows the decomposition of the light-cured polymer binder under controlled atmospheric conditions in two stages: a low temperature stage (200 °C–300 °C), leading to the evaporation of diluents with the subsequent creation of an open porosity, and a high-temperature stage, usually defined between 300 °C and 600 °C (Wang et al., 2020a). The process, associated to a relevant mass loss, leads to the formation of what is called *brown body*, exhibiting low mechanical performances and density.

Thermal debinding conditions are able to affect the quality of the final components, thus an accurate setting of process parameters as heating rate, dwelling time and sintering temperature is crucial. Upon binder decomposition at high temperature, in fact, cracks can form due to the release of carbon dioxide (CO_2) generated from polymer binder decomposition. A useful and easy strategy against delamination is to reduce the heating rate during both debinding and sintering, but it considerably lengthens the process and increases the associated energy consumption.

Current strategies to limit the above mentioned issue include the optimization of thermal profile with double vacuum pyrolysis/air debinding steps (Zhou et al., 2016), the control of debinding atmosphere (Li et al., 2020a), or even the extraction of the residual monomer by water (Coppola et al., 2022b) or CO_2 under supercritical conditions (Barry et al., 2008).

2.5 Sintering

Advanced ceramics need carefully optimized sintering cycles to obtain highly dense parts (close to the theoretical density of the material) with controlled and limited grain growth. This is one of the major challenges of advanced ceramic materials and, in the past, it has been mainly solved by two strategies. On one side, a perfect control of the raw powder (in terms of particle size and distribution, as well as packing behaviour into homogeneous, highly compact green bodies). On the other, advanced sintering technologies, such as Hot Pressing or Spark Plasma Sintering, have been adopted, in order to maximize densification while controlling the particle grain growth. When vat-photopolymerization techniques are concerned, both strategies have to face further challenges. In fact, even if a perfect distribution of particles is reached, this distribution could be hardly maintained upon addition to the resin, and the presence of the polymer fraction impede the occurrence of closely-packed green bodies. To overcome these issues, the addition of proper dispersant favouring a homogeneous dispersion of ceramic fillers into a polymer medium seems mandatory (Mohammadi et al., 2023) and the maximization of ceramic solid loading is the key to improve green and sintered density, contributing, at the same time to minimize the volumetric shrinkage (Inserra et al., 2023), as discussed in the previous paragraph.

Concerning sintering, the above-mentioned advanced techniques typically apply to dense specimens with simple geometries, and not to the complex shapes obtainable by SL and DLP.

In these regards, in order to achieve high densification degree at controlled grain size, microwave sintering, potentially applicable to any geometries and architecture, seems a promising route.

Microwave sintering represents, in fact, a valuable alternative to conventional sintering as it ideally allows to i) shorten sintering time and lower energy consumption, ii) use higher heating rates, iii) improve materials microstructure by grain refinement, as demonstrated in a recent study by Khalile and co-workers (Khalile et al., 2023) for dense and lattice 3Y-TZP samples.

Additive manufactured materials imply a further challenge during sintering, consisting on a relevant anisotropic shrinkage determined by the layer-by-layer deposition method, which could determine an increase in interlayer spacing, delamination and, consequently, geometric distortion.

Dilatometry and interrupted sintering microstructure analysis proved that this phenomenon results from a sub-optimal particle packing between adjacent printed layers, generating an anisotropic porosity distribution at the mesoscale (Manière et al., 2020).

The possibility of achieving adequate control over the anisotropy of 3D-printed ceramic components has recently aroused great interest in the scientific community.

A number of studies report how accurate control at the microstructural level through targeted selection of starting materials can be a winning strategy.

For example, a recent study by Fan and co-workers (Fan et al., 2022) showed the direct relation between microstructural anisotropy and the size of the ceramic particles dispersed within the resin. In the presence of coarse particles, ceramic components were characterized by a multilayer structure with large gaps in the horizontal direction, while appearing more uniform in the vertical one. On the other hand, by using fine powders, the rearrangement of the particles at the interface between the various layers is facilitated during sintering, favouring microstructural uniformity. This is also reflected in the mechanical anisotropy, leading to an increase in the ratio vertical to horizontal strength (σ_v/σ_h) up to 0.88.

In another study, Niu and coworkers (Niu et al., 2022) successfully managed structural and mechanical anisotropy of silica-based ceramic cores by adding proper amounts of aluminum oxide (Al_2O_3) powder. Due to the presence of alkali oxides and alkaline-earth in impurities, particle rearrangement between printing layers was significantly improved, thus providing enhanced uniformity at the microstructural level.

In recent years, several innovative methods for the prediction and tuning of structural and mechanical anisotropy of sintered parts have been proposed. Most of them are based on numerical models (Manière et al., 2020) that can be easily converted into finite element code to be eventually combined with experimental data, allowing to achieve a deep understanding of such behaviour.

Basing on this approach, Li and coworkers (Li et al., 2022b) studied the anisotropic behaviour of ceramic core samples prepared from the X, Y, and Z directions, using finite element simulation to investigate the mechanism of core delamination by modelling the slurry spreading during the printing process.

This novel approach definitely provided an effective theoretical guidance for anisotropy control in 3D printed ceramic components by vat-photopolymerization, contributing to the promotion of the technology even beyond the aerospace field.

3 Biomedical applications

Bioceramics are biocompatible materials intended to replace and restore damaged parts of the body, particularly hard tissues, such as teeth and bone.

Their mechanism of action can vary significantly depending on their composition and crystalline state, leading to a different level of interaction with biological tissues and body fluids. According to this, three different classes of bioceramics can be defined as follows (Ishikawa et al., 2003).

1. Bio-inert ceramics, chemically stable in contact with body fluids, such as alumina (Al_2O_3), zirconia (ZrO_2) and Al_2O_3/ZrO_2 composites;
2. Bioactive ceramics, able to chemically bond the host tissue without inducing any foreign body reaction, such as hydroxyapatite (HA) and bioactive glasses (BGs);
3. Bioresorbable ceramics, able to gradually resorb over time in physiological environment, leaving room for newly-formed healthy tissue, such as α-Tricalcium Phosphate (α-TCP) and β-Tricalcium Phosphate (β-TCP) and bioresorbable glasses.

Over time, a number of bioceramics has been successfully processed by SL and DLP, proving their suitability in realizing complex components with highly resolved micrometric features, controlled interaction with biological entities and cell signalling (Kim et al., 2010), in agreement with the different clinical needs.

On the one hand, it is possible to meet reproducibility and standardization requirements, resulting in a higher quality and reliability of the finished component for a safe therapeutic use, thus becoming suitable for industrial scale production and large distribution.

The second aspect, diametrically opposed, concerns the possibility of obtaining customisable products intended for advanced reconstructive applications, where the design of the object is developed and optimized on the basis of specific anatomical characteristics in order to meet both aesthetic and functional requirements.

A general overview of bioceramics vat-photopolymerization applications in medical field is provided in Figure 4.

3.1 Scaffolds for bone tissue engineering

The clinical need for bone synthetic substitutes could sound controversial considering that bone is able to self-repair and remodel, restoring its original functionality in a restrained temporal window. However, in the case of critically-sized bone defects, the implantation of 3D bone grafts is usually recommended to guide cells through regenerative pathways while providing mechanical support (Roddy et al., 2018).

Dealing with bone regeneration, great attention is addressed to the design of porous structures for trabecular bone tissue, more susceptible to structural and morphological variations upon aging and pathological states compared to cortical one (Rüegsegger et al., 1991).

In particular, in order to be selected as implantable scaffold, a porous bone substitute should satisfy a series of minimum requirements in terms of materials properties, processing and 3D structures, such as (Gerhardt and Boccaccini, 2010).

1. Biocompatibility, in order to promote cell adhesion, proliferation and synthesis of new extracellular matrix (ECM), inducing minimal immune response;
2. Bioactivity, leading to the generation of a stable bonding interface with the host tissue;
3. Biodegradability, within a time frame compatible with new bone tissue formation, avoiding the release of toxic degradation products;
4. Adequate mechanical properties, matching that of native tissue in order to adequately share mechanical loads and maintain mechanical integrity over the whole period of treatment;
5. 3D porous structure, with total porosity ≥50 vol% and open-cell architecture with interpore windows of 50–100 μm in order support cell migration, vascularization and tissue ingrowth.
6. Cost effectiveness, repeatability, reliability and scalability of the manufacturing process.

As a result, bioactive and bioresorbable ceramics such as calcium phosphates (CaPs) and bioactive glasses (BGs) are widely appreciated as grafting materials to be used in regenerative strategies due to their ability to exert osteoconductive effects, resulting in enhanced bone forming ability in a shorter healing time (Hench and Kokubo, 1998; Yuan et al., 1998; LeGeros, 2002; Kaur et al., 2014).

Compared to traditional manufacturing processes of porous ceramics, affected by poor reliability, reproducibility of results and control over relevant structural properties, vat-photopolymerization of bioactive and bioresorbable ceramics, e.g., β-TCP, HA and BGs, allows the production of precise porous structures matching bone defect geometry and exhibiting tailored mechanical properties and outstanding regenerative potential, as supported by several research studies (Bahraminasab, 2020; Martinez et al., 2022b).

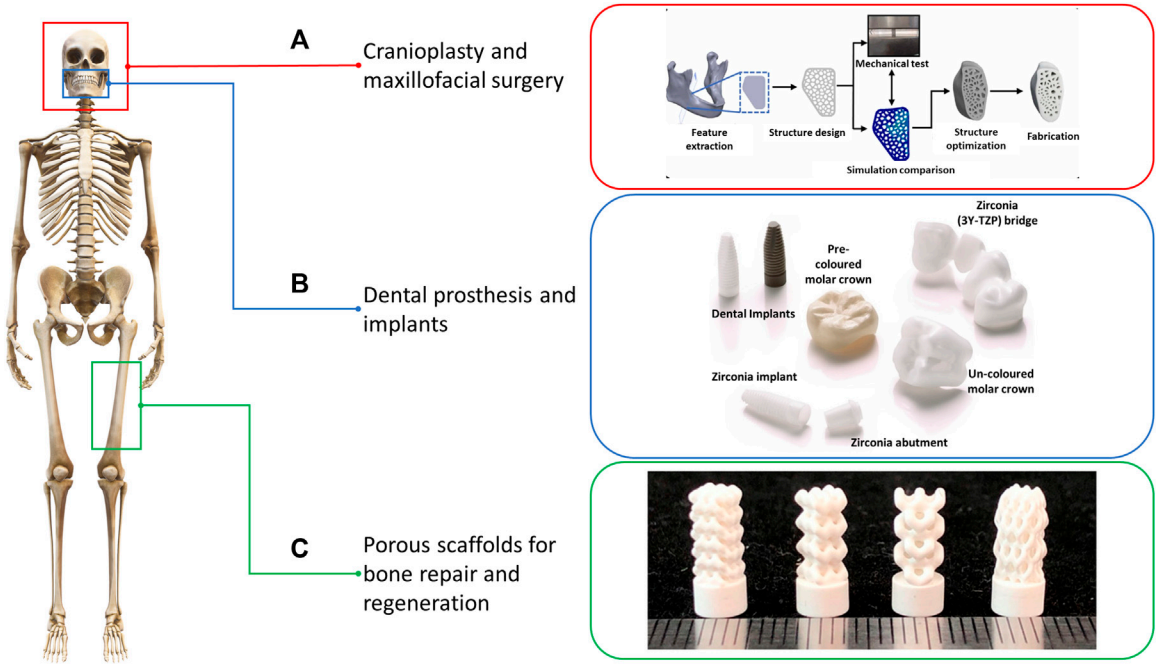

FIGURE 4
Clinical applications of vat-photopolymerization technology in medical field: **(A)** cranioplasty and maxillofacial surgery (images adapted from (Wu et al., 2022) with permission (© 2022 Elsevier Ltd.); **(B)** dental prostheses and implants (Khanlar et al., 2021); **(C)** porous scaffolds for bone repair and regeneration (Safonov et al., 2020). Images **(B)** and **(C)** adapted under the Creative Commons Attribution CC BY License.

As an example, DLP β-TCP scaffolds with hierarchical porosity and compressive strength of 17 MPa were produced by Xu and co-workers (Xu et al., 2022). *In vitro* cellular tests, performed on rat osteoblast cell line (MC3T3-E1), revealed a good capability to support cell adhesion and proliferation onto the ceramic substrate, while histological assessment confirmed the capability of these materials to support ectopic bone formation and neovascularization within a restrained temporal window (Xu et al., 2022).

In another study, Wei and co-workers (Wei et al., 2020) implanted DLP CaP-based scaffold into the dorsal muscle of adult healthy beagle dogs. Prior to *in-vivo* studies, bioactivity and *in-vitro* cytocompatibility were verified. Scaffolds clearly exhibited osteinductive and angiogenetic properties as confirmed by newly formed bone and vascular structures observed into the inner surface of scaffolds pores, with an average new bone area percentage in the ceramic implants of 1.55% ± 0.94%.

Similar results were reported by Kim and co-workers (Kim et al., 2020), who investigated the bone regenerative potential of HA/TCP DLP customized scaffolds into a dog mandibular defect model. The study revealed that the use of 3D printed scaffolds led to an improvement in bone regenerative rates compared to unfilled defect, used as negative control.

The intimate link between 3D architecture, mass transport phenomena and mechanical properties of scaffolds for bone repair and regeneration is universally recognized.

In these regards, the role of pore size, configuration and orientation (Lee et al., 2018; Liu et al., 2021b; Zhang et al., 2022a; Kang et al., 2022) on mechanical properties of CaP-based scaffold have been thoroughly investigated.

Zhang and co-workers (Zhang et al., 2022a) studied the effect of pore shape on the compressive strength and elastic modulus of β-TCP porous scaffolds. In order to do this, rhombic dodecahedron (RD), dode-medium (DM), triply periodic minimal surface (TPMS), and gyroid dodecahedron (GD) porous structures have been produced by DLP. It was found that pore configuration played a minor role in determining mechanical performances compared to the total porosity value, and scaffold with different pores shape but comparable porosity values (~80 vol%) exhibited similar compressive strength (0.4–1.4 MPa). On the other hand, when considering a specific pore configuration, mechanical properties significantly improved by decreasing the nominal porosity.

The effect of different pores configurations was reported by Kang and co-workers (Kang et al., 2022), who selected octahedral, circular, and frame design to produce HA bioactive scaffolds. Octahedral pores provided the highest bone cell proliferation and differentiation, as well as of fracture strength, corresponding to a maximum value of 5.6 ± 0.85 MPa.

On the other hand, Lee and co-workers (Lee et al., 2018) improved the compressive strength of CaP scaffolds up to 14.9 ± 1.61 MPa by opportunely tailoring pore orientation, where the highest value was observed for structures presenting frameworks oriented along the loading direction.

The effect of pore size on bioactivity and mechanical properties of HA scaffolds was selectively addressed by Liu and co-workers (Liu et al., 2021b). Structures were designed with pore size of 400, 500 and 600 μm, modelled as parallel channels and produced by SL technology. After sintering at 1,250 °C for 2h, achieving a relative density of 73%, a linear

increase of compressive strength with increasing pore size, reaching a maximum value of 38.48 MPa, was determined.

Apart from porous structure and pore size, the need to achieve sufficient mechanical strength of CaP-based 3D printed scaffolds led to investigate other factors. In these regards, within a preparatory study for the optimization of porous structures, Mohammadi and co-workers investigated the role of the HA median particle size (in the range 0.3–2.7 μm) on the formation of microstructural defects and mechanical performances of HA bulk components, allowing to identify a minimum threshold value of 0.9 μm to reach very high flexural strength (>100 MPa under optimized curing and printing conditions) (Mohammadi et al., 2023).

In another study, Zhang and co-workers, supported the use of ZrO_2 as toughening phase in HA-ZrO_2 composite scaffolds produced by DLP. In particular, the incorporation of ZrO_2 up to 6 wt% led to an overall improvement of mechanical properties by reducing the phase transformation of HA into β-TCP upon sintering, resulting in a better densification of the ceramic structure (Zhang et al., 2019).

The production of tailored biomimetic structures perfectly resembling bone features was presented as a valuable strategy to optimize multiple structural/biological aspects at once.

In these regards, an innovative approach was described by Liu and co-workers (Liu et al., 2021c) who produced trabecular like β-TCP scaffolds based on the Voronoi tessellation method. Interestingly, scaffolds with tailored pore size and porosity were manufactured on the basis of a parametric design, varying porosity from 45 to 75 vol%. In these regards, there are considerable clinical implications: the study, in fact, offers a winning strategy to precisely tune scaffolds porosity and mechanical properties within the typical porosity range of trabecular bone, taking into account all possible variation factors, including age, anatomical site, sex and bone health conditions.

A different biomimetic approach was proposed by Baino and co-workers (Baino et al., 2022), who used microtomography (μ-CT) scans of a commercial polyurethan foams to obtain a virtual 3D model suitable for the production of HA cylindrical scaffolds by DLP. In the past, foam replica method has been widely appreciated due to the possibility to obtain a faithful reproduction of the trabecular structure of the native spongy bone. However, the technique was affected by serious drawbacks in terms of mechanical performances and reliability. Compared to typical ranges of compressive strength reported for HA scaffolds fabricated by foam replica method with porosity ranging from 83% to 92% (0.37–0.5 MPa) (Gervaso et al., 2012; Muhammad Syazwan et al., 2021) the use of DLP led to significant improvement in mechanical performances up to 1.60 MPa and comparable porosity values. Moreover, intrinsic permeability value determined by acoustic pressure wave drops measurements ranged between 0.75–1.74 × 10^{-9} m^2, revealing a perfect correspondence with reference values reported for human cancellous bone.

Along these lines, vat-photopolymerization was intensively implemented to produce patient-specific components from 3D images acquired by conventional clinical imaging techniques such as computed tomography (CT) and microtomography (μ-CT) and magnetic resonance imaging (MRI). In particular, maxillofacial repair in oral and maxillofacial surgery represents one of the greatest clinical challenges of our time due to the necessity to combine aesthetic, functional and biological requirements, all fundamental for a successful therapeutic treatment of disabling bone defects (Figure 4A).

In these regards, β-TCP scaffolds with biomimetic trabecular bone architecture for large-scale mandible and crania defects repair were manufactured by Zhang and co-workers (Zhang et al., 2022a) on the basis of clinical imaging data, perfectly matching the geometry of complex mandibular and skull bone defects.

In another study, Yin and co-workers (Yin et al., 2022) optimized high mechanically stable α-TCP-based bioactive ceramic scaffolds for alveolar cleft repair, based on the fact that, compared to β-TCP, α-TCP provides faster degradation rates and exceptional bone forming ability. For this purpose, α-TCP powders doped with 6 wt% Sr were selected for the study and compared with β-TCP and undoped α-TCP scaffolds. TPMS 3D scaffolds have been designed for animal model bone repair in order to exhibit a gradient porosity, with internal pore size of 600 μm and surface pores, in contact with soft tissues, in the range of 100 μm. Authors found that Sr-doping exerted a double effect, acting both at cellular and structural level by enhancing osteoblast activity and providing structural stability in aqueous environment both *in vitro* and *in vivo* thus supporting the use of this new material for the regeneration of large bone defects.

The production of HA scaffolds with functional and structural porosity gradients was described by Wang and co-workers (Wang et al., 2020b) (Figure 5). Starting from μ-CT data, different gray values, corresponding to variable tissue porosity within the range 9.2%–94.6%, were evaluated, using Matlab for numerical calculation and statistical analysis. The scaffolds exhibited high compressive strength, in the range 5.6–18.4 MPa, with elastic modulus between 2.4–5.9 GPa, in good agreement with reference values reported for human trabecular bone. In perfect analogy with biological systems, characterized by the arrangement of Volkmann and Haversian canals, it was found that pores orientation played a major role in determining the mechanical performances of the porous structure. In particular, authors observed how the presence of horizontal pores negatively affected compressive strength of the scaffold.

Compared to bioceramics of second generation such as stoichiometric HA, BGs are characterized by higher reactivity in contact with body fluids, leading to faster formation of bonding interfaces with host tissue and, as a direct consequence, higher new bone formation rates *in vivo*. Moreover, their ability to activate beneficial cellular pathways by the action of ion dissolution products resulting from their bioactive mechanism, have been extensively demonstrated (Oonishi et al., 2000; Varanasi et al., 2017). As opposed to exceptional bioactivity in contact with body fluids, BG-bases porous structures are typically affected by low mechanical strength and fracture toughness, resulting in a poor reliability of the implant in load bearing applications. Moreover, most of manufacturing technologies described in literature suffer from poor reproducibility and standardization levels. As a direct result, BG-based scaffolding technology is still limited to laboratory practice, without an effective translation to clinical application (Gerhardt and Boccaccini, 2010; Baino et al., 2019; Fiume et al., 2021).

SL and DLP technologies can make a difference, providing an effective contribution in closing the gap between laboratory practice and clinical application of BG-based bone grafts allowing to tailor

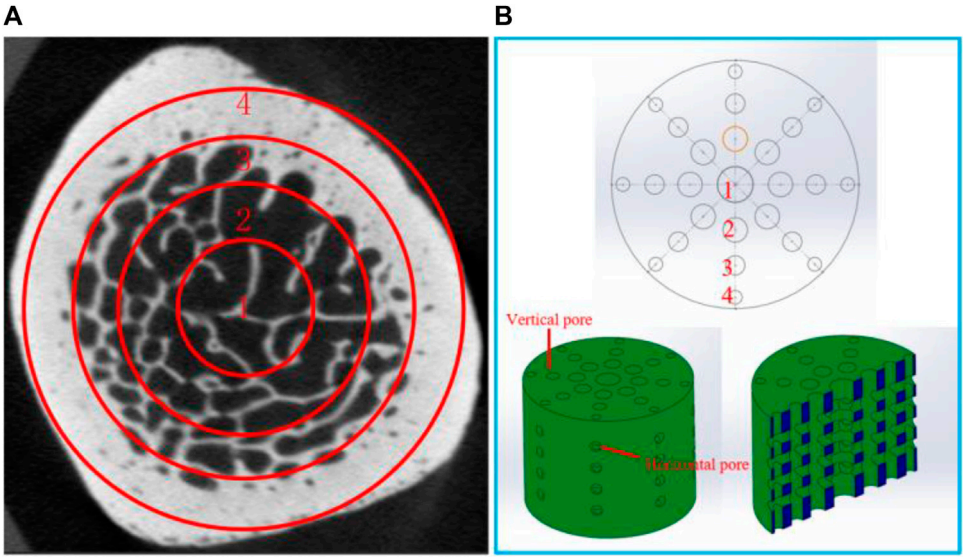

FIGURE 5
Design of biomimetic HA scaffolds with gradient porosity: from μ-CT clinical imaging **(A)** to customized CAD model **(B)**. Image reproduced from (Wang et al., 2020b) under the Attribution-NonCommercial-NoDerivatives 4.0 International (CC BY-NC-ND 4.0).

mechanical properties of the scaffold at a preliminary stage. In these regards, Gmeiner and co-workers (Gmeiner et al., 2015) demonstrated the suitability of DLP in optimizing mechanical properties of both solid bulk component and porous scaffolds based on the 45S5 system, achieving biaxial bending strength up to 124 MPa, close to the reference values reported for natural cortical bone. Moreover, it was found that mechanical properties of bioactive glass porous scaffold were improved by performing pre-sintering treatments on glass powders to decrease volume shrinkage upon sintering, thus improving the dimensional stability of the scaffold.

Among the major challenges to be tackled in the coming years, certainly the possibility of controlling and regulating the degradation rates of bioactive and bioresorbable scaffolds stands out as a key element in taking these scaffolds to a new level. In this regard, the study conducted by Su and coworkers (Su et al., 2022) on the DLP-based production of gyroid-structured ternary composite scaffolds (biphasic calcium phosphate (BCP) and 45S5 bioglass® (BG)) is particularly interesting. In particular, the study revealed a beneficial reactivity between bioactive glasses and BCP, leading to the formation of active crystalline phases $CaSiO_3$ and $Na_3Ca_6(PO_4)_5$ responsible for accelerated the exchange rate of Si^{4+}, Ca^{2+}, and PO_4^{3-} with HCO^{3-} in simulated body fluids (SBF) and resulted in the rapid formation of carbonated hydroxyapatite with a petal and needle-like morphology, enhancing cell adhesion and proliferation. Tunable degradation rates were obtained by varying the BG content. In a similar manner, a dependence between the BG content and compressive strength was found, showing an increasing trend by increasing the BG content from 20 to 60 wt%, reaching a maximum value of 1.29 MPa.

Although bioactivity is one of the fundamental requirements for the realisation of a scaffold for bone regeneration, it is sometimes advisable to favour structural requirements, promoting the establishment of a chemical bond with the surrounding tissue through alternative strategies involving the use of bioactive coatings deposited on an inert ceramic substrate characterised by superior mechanical properties.

In these regards, Coppola and co-workers (Coppola et al., 2022a) developed ZrO_2-based DLP scaffolds with lattice and trabecular-like structures (Figure 6 a-b). Scaffolds sintered at 1,400 °C for 1 h achieved superior mechanical properties compared to typical bioactive ceramic scaffolds, with a flexural strength up to 177 MPa and 34 MPa for lattice and trabecular structures, respectively. The post-application of a bioactive CaP coating on the surface by dipping (HA:20 wt%) and subsequent calcination at 1,300 °C (Figure 6 c-d) led to the formation of a biphasic HA/β-TCP layer, able to provide bioactive properties to the scaffolds upon immersion in SBF up to 14 days at 37 °C. Interestingly, trabecular structure, characterized by the presence of convex surfaces and a more complex geometry, led to a higher degree of covering compared to lattices (Figure 6 e-f). This can be attributed to static SBF testing conditions which hindered the dispersion of ions released from the coating and resulting in higher concentration of Ca^{2+} and HPO_4^{2-} species inside the lattice pores compared to the surface.

Similar results were reported by Zhang and co-workers (Zhang et al., 2021a) who investigated the effect of calcium silicate/HA coating composition on the mechanical properties and bioactive behaviour of ZrO_2 porous scaffolds produced by DLP. Increasing content of calcium silicate within the coating led to a significative improvement in mechanical properties with a total increase in compressive strength of 68% when pure calcium silicate coatings are considered. After immersion in SBF, a decrease in compressive strength was observed compared to as-produced coated-scaffolds, but still within suitable ranges for applications in load bearing anatomical sites.

Safonov and coworkers (Safonov et al., 2020) developed parametric 3D models of cylindrical Al_2O_3 bone implants characterized by a complex cellular microstructure and fabricated by SL starting from commercial photocurable pastes (Figure 4C). Single axis compressive tests were performed, where maximum load

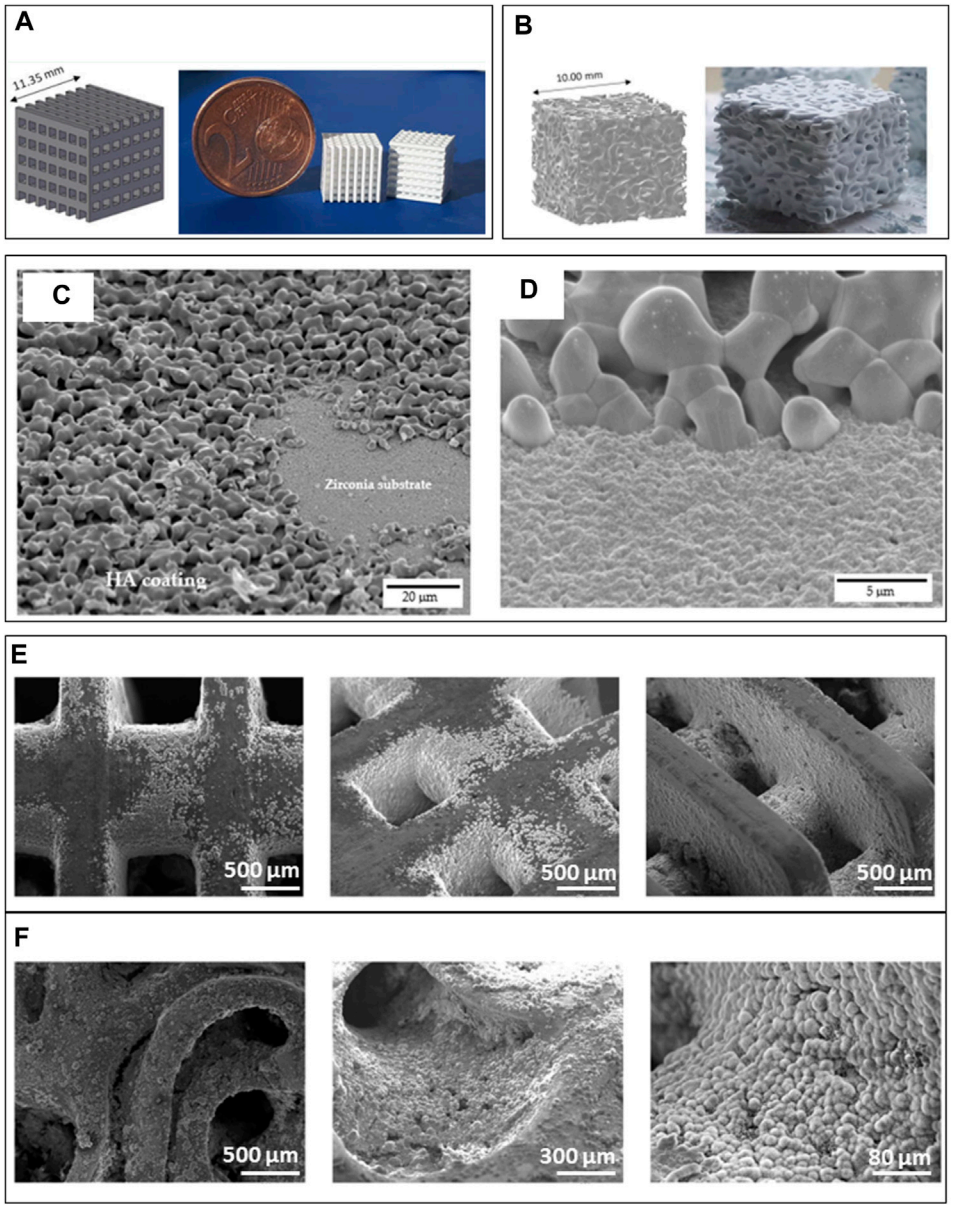

FIGURE 6
ZrO_2-based DLP scaffolds with lattice **(A)** and trabecular-like structures **(B)**; FE-SEM cross-sectional micrographs showing the interface between 20% HA coating and zirconia scaffold at different magnifications **(C–D)**; FE-SEM micrographs showing HA coated lattice **(E)** and trabecular **(F)** scaffolds surface after 14 days immersion in SBF. Image adapted from (Coppola et al., 2022a) under the Creative Commons Attribution CC BY License.

for tested samples ranged between 93 and 818 N, depending on the size of the unit cell and the trabecular thickness. In this way it could be ideally possible to precisely design cellular structures basing on specific mechanical requirement, to be defined according to the anatomical site, the state of health of bone tissue, as well as the age and the sex of the patient.

In recent years, there has been growing interest in the development smart scaffolds exhibiting, just like native bone, piezoelectric properties, capable of stimulating tissue ingrowth by reproducing the tissue's electrical microenvironment (EM) (Chen et al., 2023).

In these regard, DLP technology was successfully used by Jiang and coworkers (Jiang et al., 2022) to shape porous $BaTiO_3$ piezoelectric scaffolds with maximum bending strength of 57.9 MPa and the relative density of 94.2%. Interestingly, scaffolds exhibited tunable mechanical and electrical properties according to the porosity content. In particular, finite element methods showed that by increasing the porosity, the potential of porous scaffolds $BaTiO_3$ piezoelectric ceramics become more uniform.

3.2 Dental restoration and implants

At present, computer-aided design and manufacturing technologies (CAD and CAM) based on subtractive approaches represent the gold standard in dental prosthetics. However, these technologies suffer from a number of limitations that are partly

responsible for the high cost, as well as for the considerable waste of material, with inevitable consequences at economical/environmental level (Bindl and Mormann, 2005; Wang et al., 2008; van Noort, 2012).

In these regards, a complete switch to additive manufacturing techniques would bring great benefits, pushing materials engineers, biomedical engineers and dentists to actively collaborate to make vat-photopolymerization technologies available for the clinical-scale manufacture of dental components. However, there are several aspects to be considered, including productivity, delivery time, dimensional tolerance, mechanical and aesthetic properties (Li et al., 2020c). Apart from practical aspects, most of these requirements rely on the accurate selection of raw materials to be used as basic components within the photocurable resin, determining not only the mechanical and physical properties of the finished component, but also the printing efficiency.

Among biocompatible structural ceramics, high-purity α-Al_2O_3 (≥99.99%), tetragonal zirconia polycrystal (TZP) stabilized with Y_2O_3 (Y-TZP) or CeO_2 (Ce-TZP), or MgO partially stabilized ZrO_2 (MgO-PSZ) (Chevalier and Gremillard, 2008), as well as their composites (Piconi and Sprio, 2021; Shekhawat et al., 2021), have been extensively studied for both dental and orthopedic use due to their exceptional biocompatibility, superior mechanical properties and high corrosion resistance, which make them materials of choice in the production of load bearing components subjected to cyclic loads, as it occurs upon mastication (Studart et al., 2007) or in correspondence of articulating surfaces (Bergmann et al., 2016).

Although in the orthopedic field there are concerns about the use of ZrO_2-based ceramics due to the failure of Y-TZP femoral prosthetic components determined by low-temperature degradation (LTD) phenomena (Chevalier et al., 2009), in the dental field, Al_2O_3, ZrO_2 (especially 3Y-TZP) and their composites are all considered eligible materials to be used both in the fabrication of endo-osseous implants, abutments, dental crowns and bridges (Figure 4B).

To date, open challenges related to the photopolymerization of ceramic slurries for dental applications concern delamination issues (Li et al., 2019), volumetric distortions (Revilla-León et al., 2022; Denis et al., 2023), surface quality and aesthetic requirements, as summarized in Figure 7.

Most of challenges reported are directly related to the layer-by-layer deposition approach, relying on the use of printing supports (Park et al., 2019), as well as to the debinding process required to remove the polymeric binder phase, inducing anisotropic volumetric shrinkage along the *X*, *Y* and *Z*-axis.

Indeed, components produced by subtractive technologies are characterized by high density values and isotropic shrinkage in space, allowing to achieve high levels of geometric accuracy of the component compared the original model.

Dehurtevent and co-workers (Dehurtevent et al., 2017) compared physical and mechanical properties of Al_2O_3 dental crown frameworks fabricated by vat-photopolymerization technologies and traditional manufacturing methods based on subtractive approaches. Suitability of dental crowns for clinical use relies on high flexural strength, which should be higher than 300 MPa and good structural reliability, assessed by Weibull modulus and characteristic strength. In particular, the higher the Weibull modulus, the greater the homogeneity of the components, indicating small variations in terms of flexural strength. Despite anisotropic shrinkage was observed, the comparative evaluation of vat-photopolymerization and traditional subtraction-based technologies definitely supported the possibility to additively produce dental crowns suitable for clinical application *in vivo*, provided that the rheological properties of photocurable ceramic slurries are optimized in terms of solid loading and particle size, identified as 75–80 wt% and 1.56 ± 0.04 μm, respectively.

The same issue was addressed by Revilla-León and co-workers (Revilla-León et al., 2022) about manufacturing accuracy and volumetric changes of ZrO_2 components exhibiting variable porosity values, i.e. 0, 20 and 40 vol%. Kruskal–Wallis test and Mann-Whitney U test revealed significant differences among the 3 groups considering both single and pairwise comparison in length, width, and height ($p < .001$). Even in this case, all the tested groups exhibited non-uniform volumetric changes, where the highest value was observed along the *Z*-axis, corresponding to the printing direction. Interestingly, it was found that printing accuracy and volumetric variations increased and decreased respectively with the increase of porosity value. Despite this, even the sample exhibiting the highest porosity presented a faithful geometry compared to the virtual 3D model.

In another study, Meng and co-workers (Meng et al., 2022) systematically investigated the influence of curing parameters and shrinkage ratios of a photocurable ceramic resin based on 3Y-TZP with an average particle size of 0.2 μm, evaluating dimensional accuracy and crown fit for potential use in clinical applications. Spatial resolution of green ceramic components fabricated by vat-photopolymerization relies on multiple factors, affecting in turn the quality of the sintered component. Enlargement factors for ZrO_2 fixed crowns with a fired density of 6.01 ± 0.02 g/cm^3 were respectively 1.400, 1.400 and 1.500 along the *X*, *Y* and *Z*-axes. Although crown fit of ZrO_2 fixed crown almost matched clinical standards, with an internal fit of 239.3 ± 7.9 μm (reference value: ≤300 μm) and marginal fit of 128.1 ± 7.1 μm (reference value: ≤120 μm), an additional critical aspect was related to the use of support structures for the printing, inevitably affecting the geometrical fidelity of the component due to the intrinsic difficulties in their complete removal. In these regards, Lian and co-workers (Lian et al., 2018) optimized a three-part auxiliary support applied to the occlusal surface of molar crown bridges, obtaining an average dimensional error of the green body of 150 μm.

A solution to this problem was provided by Li and co-workers (Li et al., 2022e), who produced integrated 3Y-TZP ceramic crown using viscoelastic paste-based vat-photopolymerization with a conformal contactless support including a top conformal structure without any contact with the crown and appropriate empty layer. The final component exhibited good geometrical accuracy with a deviation of 40–70 μm from the virtual model, as well as outstanding flexural strength of 1,117 MPa and fracture toughness of 7.76 MPa·m$^{1/2}$.

Large amount of residual ZrO_2 produced by manufacturing processes involved in the realization of dental components can be efficiently managed by reintroducing them into the production cycle as a base material for the development of light-cured ceramic resins based on waste material, with great benefits in terms of costs. The feasibility of this "green" approach was investigated by Su and co-workers (Su et al., 2020) comparing pristine or recycled ZrO_2 powder for the realization of

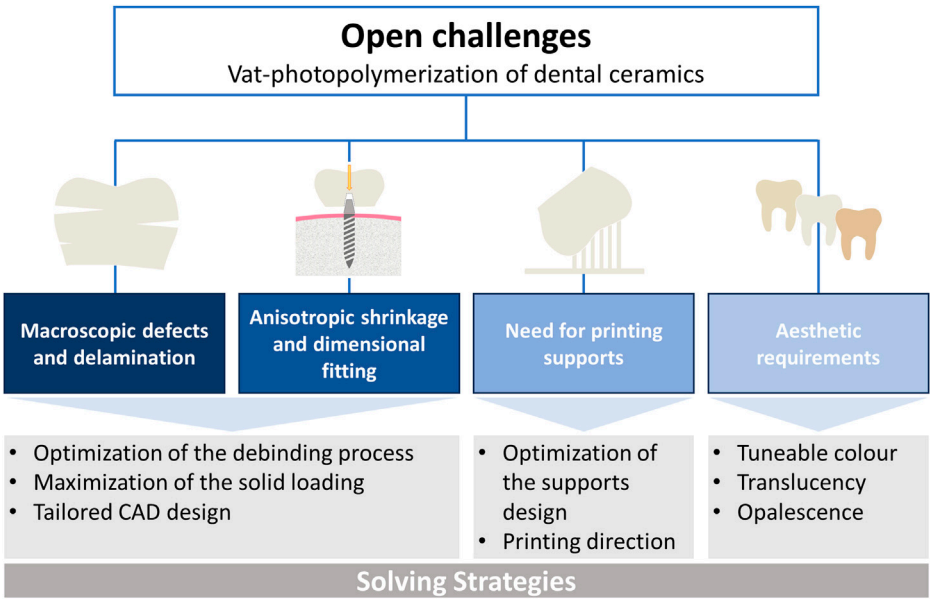

FIGURE 7
Overview of open challenges and main solving strategies for the optimization of ceramic dental components fabricated by vat-photopolymerization technologies.

dental crowns. The characteristics of pristine ZrO_2, recycled powder, and as-prepared resins were examined. Pristine powders exhibited a smaller particle size of 0.2 μm compared to recycled powders (2.9 μm). Both pristine and recycled powder were characterized by the presence of tetragonal and monoclinic phase, where the fraction of tetragonal ZrO_2 considerably increased after recycling passing from 26.9% to 67.9%. Overall, considering a layer thickness of 40 μm the use of recycled powders leads to a deterioration of the mechanical and physical properties of the part, with a reduction in density from 99% to 90% and flexural strength from 874 ± 136 MPa to 389 ± 24 MPa. However, concerning geometrical accuracy, both the powders led to acceptable tolerance level below 100 μm, which is the maximum admissible for clinical use, but even in this case, the use of recycled powders produced the greatest error, ranging from 42.1 to 92.6 μm, while the error resulting from pristine powder was found to be within the range 36.8–74.5 μm.

Improved mechanical properties in terms of crack propagation and fracture toughness of prosthetic elements can be obtained by the production of ZrO_2-Al_2O_3 bio-ceramics, namely, Al_2O_3-toughened ZrO_2 (ATZ) and ZrO_2-toughened Al_2O_3 (ZTA). While Al_2O_3 contributes in improving hardness and wear resistance, the main contribution of the ZrO_2 phase relies on the transformation toughening mechanism, providing toughness and reliability (Hannink et al., 2004).

ATZ and ZTA mechanical and microstructural properties were investigated by different research groups all over the world (Wu et al., 2017; Wu et al., 2018; Schwarzer et al., 2019; Xing et al., 2020a; Borlaf et al., 2020; Liu et al., 2020; Zheng et al., 2020), confirming the suitability of these materials for dental restoration and implants in terms of both mechanical and biological properties.

As an example, Chen and co-workers (Chen et al., 2021a) produced DLP ZrO_2-Al_2O_3 ceramics with a relative density, Vickers hardness and fracture toughness of 99.09%, 16.66 GPa and 6.88 MPa·$m^{1/2}$, respectively. Similar results were reported by Nevarez-Rescon and co-workers (Nevarez-Rascon et al., 2009) for composites with 20 wt% Al_2O_3, 80 wt% 3Y-TZP, with hardness of 16.05 GPa and maximum fracture toughness 7.44 MPa $m^{1/2}$.

In another study, Coppola and co-workers (Coppola et al., 2021) fabricated by DLP dense Al_2O_3, ZrO_2 and composites with increasing ZrO_2 content (15, 50 and 85 vol%), demonstrating the existence of a well-defined microstructural-properties relationship. In particular, by increasing the ZrO_2 volume content, density increased from 95% to 99% for components sintered at 1,500 °C. On the other hand, hardness values increased from 15 to 21 GPa by increasing the Al_2O_3 volumetric fraction, according to the rule of mixture for the evaluation of composite materials properties. In these regards, best performances were associated to the composite with 15 vol% Al_2O_3 content.

In recent years, great attention was addressed to the optimization of ceramic composites for dental restoration based on ceria (CeO_2) as stabilizer of the zirconia tetragonal phase. Compared to 3Y-TZP, Ce^{4+} enters the ZrO_2 lattice without creating oxygen vacancies, responsible for degradation in moisture environments which could led to the formation of cracks, compromising the long-term durability of the implant. Moreover, the larger mismatch in Ce-TZP and Al_2O_3 refractive indexes is responsible for improved opalescence of composite surface compared to Y-TZP-based ceramic (Shiraishi and Watanabe, 2016).

In a recent study Inserra and co-workers (Inserra et al., 2023) investigated the printability of Ce-ZrO_2/Al_2O_3 by DLP by optimizing different resin compositions on the basis of ceramic solid load and dispersant amount. The sintered composites were characterized by a homogeneous phase distribution, showing high

density values between 98.3% and 99.4%. Tetragonal phase was completely retained after sintering, while on the fracture surface a 78 vol% of monoclinic phase was observed, indicating that an effective stabilization of the tetragonal phase could be achieved by adding 11 mol% CeO_2 as stabilizer, and at the same time the correct transformation toughening mechanism was active.

Besides the pinning effect exerted by Al_2O_3 phase on ZrO_2 grains, the addition of elongated phases to bi-phasic materials, such as strontium hexaluminate ($SrAl_{12}O_{19}$), could further improve the fracture toughness of the material by a crack deflection mechanism. In these regards, innovative ZrO_2-based composites, based on equiaxial α-Al_2O_3 and elongated $SrAl_{12}O_{19}$ phases dispersed in a CeO_2-stabilized ZrO_2 matrix have been optimized by Palmero and co-workers (Palmero et al., 2015) for reliable use in dental field. A new synthesis process based on a wet-surface coating route, patented in 2018 (Montanaro et al., 2018), allowed to obtain homogeneous microstructural features resulting in metal-like mechanical reliability (Weibull modulus ~60) of ceramic components with 10.5 mol% CeO_2 fabricated by cold isostatic pressing, achieving a biaxial bending strength of 1.1 GPa and fracture toughness higher than 10 MPa$\sqrt{m}$ (Reveron et al., 2017).

In a recent study by Fournier and co-workers (Fournier et al., 2023), the same compositional system was used as basic material for DLP, investigating the effect of processing parameter on the ductile behavior and transformability of the composite materials. Three phasic ceramic composites with composition 84% 11Ce-TZP, 8% α-Al_2O_3 and 8% $SrAl_{12}O_{19}$ were processed using a curing laser wavelength of 405 nm to the domain of high UV absorption of Ce-TZP powders. Ceramics with high density (~99%) and mechanical properties suitable for possible use in dental and maxillofacial applications were obtained. However, in comparison with components produced by cold isostatic pressing, a slight deterioration in mechanical properties was observed, which also resulted in a greater variability in mechanical strength, attributed to the formation of long cracks observed along the entire volume of the sample.

Besides mechanical properties and geometrical fidelity, aesthetic requirements play a pivotal role in the manufacturing of dental crowns and bridges. Optical properties of ceramic samples are mostly influenced by microstructural features and material porosity and high-density values produce beneficial effects on the aesthetic properties of the prosthetic component. In these regards, the use of vat-photopolymerization to produce ZrO_2-based ceramics could lead to some limitations due to the opacity of the material (Shahmiri et al., 2018). Moreover, layer-by-layer deposition strategies are typically associated with lower relative density values than traditional manufacturing processes. Furthermore, Shiraishi and co-workers (Shiraishi and Watanabe, 2016) demonstrated the influence of sample dimensions on light transmittance, translucency and opalescence of Ce-TZP/Al_2O_3 composite materials, determining a negative correlation between translucency/opalescence parameters and sample thickness. As a consequence, the formation of cracks and defects such as internal pores and agglomeration within the material has to be avoided.

As previously mentioned, common optimization strategies for aesthetic properties rely on the maximization of solid loading.

In these regards, Jung and co-workers (Jung et al., 2023) optimized 50 vol% 5Y-PSZ ceramic suspensions to confer high flexural strength and translucency properties to dental crowns fabricated by DLP (Figures 8A–C), using a layer thickness of 50 μm and an exposure time of 3 s. The process allowed obtaining highly dense (99.03% ± 0.39%) components characterized by high flexural strength (625.4 ± 75.5 MPa) and % transmittance (31.4 ± 0.7).

Moreover, the combination of an accurate design of the 3D model, combined with optimized exposure parameters resulted in a very high dimensional accuracy with an RMS for marginal discrepancy = 44.4 ± 10.8 μm and RMS for internal gap = 22.8 ± 1.6 μm (Figure 8 d-e).

In another study, Xiang and co-workers (Xiang et al., 2021) investigated the effect of printing direction (horizontal and upright) on different physical and mechanical properties. Interestingly, the study revealed that by varying the building direction, optical properties of the material can be optimized. In particular higher translucency was obtained by building samples in upright fashion, as this direction induced fewer internal defects, reaching a relative density of 95.4%.

Another strategy implies the addition of PEG200 as plasticizer agent within the resin composition, which was effective against defects formation, significantly enhancing flexural strength of ZrO_2 dental components from 302 ± 15 to 1,150 ± 25 MPa (Han et al., 2023).

Color-related aesthetic features can be opportunely adjusted by adding doping oxides in order to reproduce the complete color palette of the natural tooth, subject to large variations related to age, state of health, eating habits and lifestyle.

In these regards, Fe_2O_3 was successfully used as dopant for dental 3Y-TZP ceramics fabricated by vat-photopolymerization strategies (Wang et al., 2023b), demonstrating the possibility to change the color from white to yellow in a controllable way. However, Fe_2O_3 addition led to relevant changes also in the microstructural properties of the component, leading to the transition from tetragonal to monoclinic phase, reducing the intrinsic toughening effect. Furthermore, a decrease in hardness value was observed by increasing the dopant content due to the entrance of Fe^{3+} ions within the ZrO_2 matrix, creating oxygen vacancies. Despite a negative effect of iron oxide on mechanical properties was observed, flexural strength of doped-samples was still within the reference ranges for clinical applications, validating the approach for the production of colored ZrO_2 crowns and bridges meeting aesthetic requirement for natural tooth replacement in a wide chromatic range.

Literature search highlights the intensive use of ZrO_2-based materials for the production of dental crowns and bridges, but there is little published data on endosseous ZrO_2-based screw implants shaped by vat-photopolymerization technologies. A possible reason could be the tendency for cracks to develop, which could compromise the durability of the implant, making it necessary a second surgery, definitely more invasive than replacing a dental crown or bridge (Kontonasaki et al., 2020).

3.3 Ceramic SL and DLP in medical field: relevant outcomes and final considerations

SL and DLP exert a great deal of fascination in the biomedical field, and this is mainly due to the possibility of addressing individuality requirements characteristic of each specific clinical case. The studies reported are clear examples of how the scientific

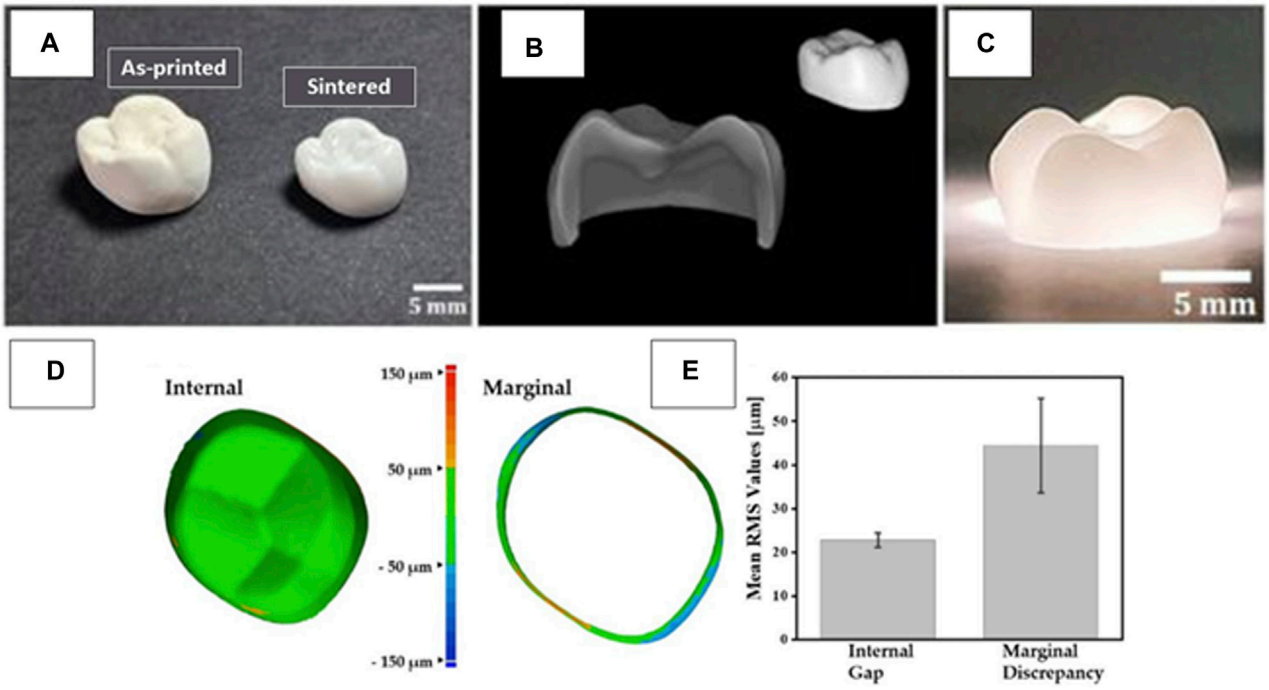

FIGURE 8
Optical image showing as-printed and sintered dental crowns **(A)**; µ-CT image of a sintered dental crown **(B)**; optical image showing translucency of a sintered dental crown under light illumination **(C)**; color maps generated by superimposition of scanned data of a 5Y-PSZ dental crown **(D)** and original CAD data and measured mean RMS values for marginal discrepancy and internal gap **(E)**. Image adapted from (Jung et al., 2023) under the Creative Commons Attribution CC BY License.

community is devoting considerable efforts to the transfer of this technology into clinical practice in various fields of application, such as orthopedics and dentistry, the most representative dealing with bioceramic materials.

However, considering these two applications, there are different considerations to be made according to the requirements to be met.

In particular, concerning scaffold manufacturing for bone replacement.

- The introduction of vat-photopolymerization based strategies led to an undeniable progress compared to traditional manufacturing technologies. In this case, in fact, the high reproducibility of the process is potentially enough for standardized mass-produced porous grafts, eventually available in different size and geometries.
- The possibility to produce patient-specific scaffolds and customized implants is highly promising but additional dedicated studies aimed at the definition of clear standards for slurries formulation, printing parameters and sintering treatments are required;
- Further steps must be taken for a complete translation of scaffolding technologies to clinical practice. This is actually imputable to various causes, related both to materials processing and some relevant and still unsolved regulatory issues concerning their validation and use in clinical practice.

On the other hand, considering dental restoration approaches.

- Results in the field of dental prosthetics are promising but still not sufficient to justify a complete switch to AM techniques.
- Relevant issues deserve improvement, such the accuracy of 3D printed zirconia fixed dental prostheses, which is not that high as the one provided by subtractive manufacturing approaches, currently representing the golden standard.
- Advantages that would result from a complete transfer to vat-photopolymerization technologies should be the guiding force for further exploration in this field in the next future.

4 Energy and environmental applications

Ceramics are gaining increasing success for energy and environmental applications, where materials are typically exposed to harsh environments, such as high temperatures or corrosive conditions. Ceramics show a combination of unique features, such as refractoriness, thermal shock resistance, chemical stability, corrosion and oxidation resistance, strength, low density and–in some cases–low cost (Labhsetwar et al., 2012; Cramer et al., 2022). This unique set of properties makes ceramics to exceed metal or polymer-based materials performance, and to play a key role in the development of sustainable energy and mitigation of environmental issues (Chen et al., 2021b).

The exponential growing of the renewable energy sector (Jaeger, 2021), as the opposite trend to the massive use of fossil fuels, is well

justified by the increasing implementation of hydrogen-based technologies (Ruiz-Morales et al., 2017). Hydrogen can be produced from renewable energies by photocatalytic water splitting (Ni et al., 2007) or through thermolysis using concentrating solar powder (Steinfeld, 2005), as well as by the traditional natural gas (Boretti and Banik, 2021) and methanol (Iulianelli et al., 2014) reforming methods. Once produced, hydrogen can be stored in several types of materials, to be used afterwards for providing power through Solid Oxide Fuel Cells (SOFCs) (Ruiz-Morales et al., 2017).

Advanced ceramics are successfully used in most of the above-mentioned technologies, where the tuning of their composition and micro/macro-structure is a mandatory step to achieve the expected exceptional properties. In fact, the design of these ceramics can critically affect parameters like performance, stability, reactivity (gas flow-paths to/from the reaction sites, for example,) (Ruiz-Morales et al., 2017). 3D printing technologies allow unprecedented designs, while reducing the production costs by limiting waste, and simplifying the manufacturing by reducing the number of fabrication steps (assembly and machining). Some examples related to the implementation of hydrogen-based technologies through vat-photopolymerization techniques are described in the following.

A first example is provided by Wang and co-workers (Wang et al., 2021), who exploited the DLP technology for building a reactor aimed at the methanol conversion into hydrogen. Specifically, the γ-Al_2O_3 catalyst career was printed, where the device was designed with two differing channel size. The former was characterized by 600 μm channel and 300 μm strut sizes, while in the second design the channel size was decreased to 300 μm. The printed parts were sintered at 750 °C, as this temperature corresponded to the best compromise between sufficient mechanical strength and negligible phase transformation of the γ-Al_2O_3 phase into α-Al_2O_3, not to decrease the career specific surface area. The sintered parts were then submitted to impregnation into a zinc nitrate/copper nitrate solution, followed by drying and calcination under hydrogen atmosphere at 450 °C for 4 h. To test the methanol conversion into hydrogen, a methanol aqueous solution was sent to the reactor at different flow velocities, and the gas produced was analysed by a gas chromatography. The catalyst with a smaller pore size showed slightly higher conversion, as the smaller diffusion radius probably induced a larger contact area.

Once produced, hydrogen can be successfully converted into electricity by means of SOFCs (Pesce et al., 2020) whereas Solid Oxide Electrolyte Cells (SOECs) run in regenerative mode, producing hydrogen again. In both cases, these electrochemical cells are made by multilayer ceramics, consisting of a gas-tight oxide-ionic conductor electrolyte as the core thick layers, and the two electrodes as the side, thin layers. The state-of-the-art material for the electrolyte is 8 mol% yttria-stabilized ZrO_2 (YSZ); for the cathode (oxygen electrode), lanthanum strontium manganite/YSZ composite (LSM-YSZ) is typically used, while Ni–YSZ cermet is the common anode (fuel electrode) material (Pesce et al., 2020). In spite of such well-consolidated compositions, continuous efforts are dedicated to develop new materials to increase the performance of the device, as well as to mitigate the concerns over materials supply (i.e., reduction of rare Earth metal content). On the opposite, the role of the cell geometry on the hydrogen conversion has been scarcely investigated. Cell configurations are currently limited to the planar and tubular ones, fabricated by tape casting and extrusion technique, respectively (Masciandaro et al., 2019). 3D printing technology opens new possibilities, for instance by designing complex geometries, especially for the electrolyte, able to increase the active area of the cell and consequently the performance (Pesce et al., 2020).

In this frame, Masciandaro and co-workers (Masciandaro et al., 2019) used SL to print SOFCs with two different configurations: a planar and a thinner honeycomb 3 YSZ electrolyte membrane, this second designed to have a higher surface area compared to the planar one. For both configurations, self-supported membranes were built, consisting of monoliths made by the YSZ membranes integrated with supporting rings, with the aim of avoiding gas leakage. The 3D printed 3 YSZ pieces were sintered at 1,450 °C/2 h. Then, commercial NiO–YSZ and LSM–YSZ pastes were separately applied on the membranes, and sintered again. The performance of the cells was evaluated under water saturated pure hydrogen (fuel electrode) and synthetic air (oxygen electrode) atmospheres, between 800 °C and 900 °C. The honeycomb-like configuration provided increased power density compared to the planar one, where the enhancement was entirely imputed to geometrical aspects.

A similar approach was used by Pesce and co-workers (Pesce et al., 2020) who used SL to print planar and corrugated YSZ electrolytes, where the latter configuration was designed to increase up to 60% the active cell area. Again, self-standing membranes were built, with the YSZ layer on the top or a connected ring. The YSZ membrane was sintered at 1,300 °C for 4 h, achieving high densification degree as required to ensure the electrolyte gas tightness. The electrodes were fabricated by painting commercial NiO–YSZ and LSM–YSZ pastes on the 3D printed and sintered YSZ pieces. Specifically, as reported above, NiO-YSZ was used as the anode (fuel electrode) and sintered at 1,400 °C/3h, while the cathode made by LSM–YSZ (oxygen electrode) was sintered at 1,200 °C/1 h. The cells were tested under both SOFC and SOEC configurations: in the former case, under hydrogen (fuel electrode) and synthetic air (oxygen electrode) atmospheres, between 800 °C and 900 °C; in the latter, a mixture of steam and CO_2 was converted into syngas (CO and hydrogen) by current injection at 900 °C. The performance of the corrugated devices (in both SOFC and SOEC configuration) was 57% higher than the planar ones, in a fair agreement with the surface area increase.

In Figure 9, examples of the new membrane configurations (honeycomb on the top, and corrugated on the bottom right (Masciandaro et al., 2019; Pesce et al., 2020), compared to the traditional planar one (bottom left) are displayed. In all cases, membranes are monolithically integrated with the supporting rings, as allowed by 3D printing technologies.

A further improvement was provided by the work of Jia and co-workers (Jia et al., 2022) who succeeded in the fabrication of SOCFs stacks still using SL. Conventional stacks manufacturing consists on the fabrication of the single cells and their assembly through multiple interconnections and joints: the process is complex, time-consuming and implies different uncertainties that limit its industrialization. Furthermore, the different materials used into the joints are characterized by different thermal expansion coefficients from the main SOFC material, decreasing stability, reliability and

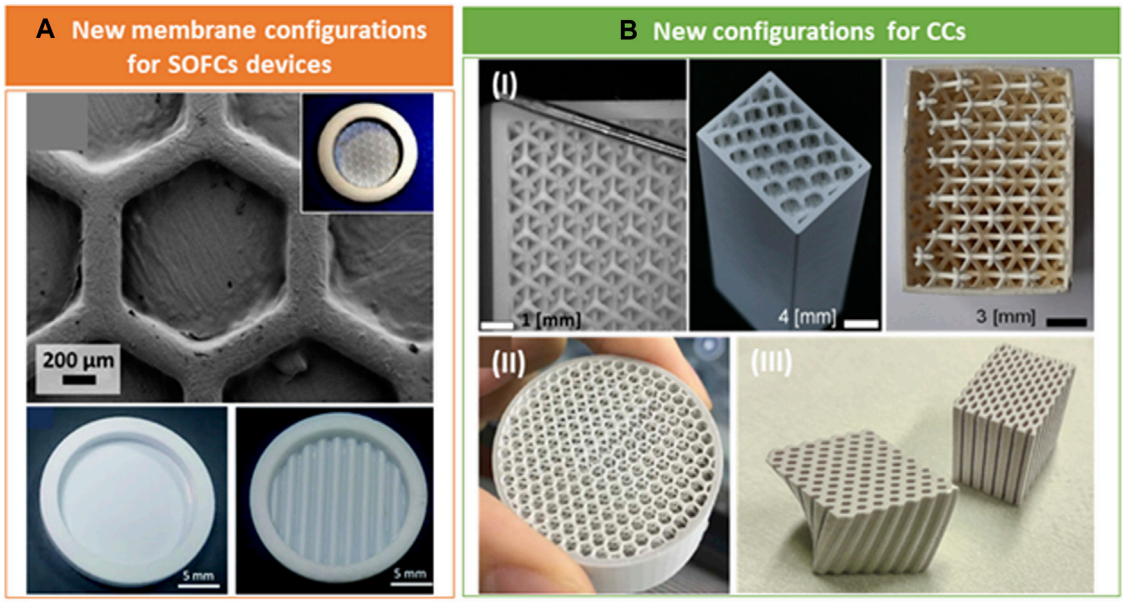

FIGURE 9
(A) New membrane configurations for SOFCs. Top: SEM micrograph of a 3D printed membrane with honeycomb structure (adapted from (Masciandaro et al., 2019) with permission (© 2017 Elsevier Ltd.); Bottom: self-standing membranes with planar (left) and corrugated (right) configurations (adapted from (Pesce et al., 2020) under the Creative Commons Attribution 3.0 Unported Licence). **(B)** New configurations for CCs **(I)**: rotated cube-based structure after 3D printing (left), sintering (centre) and washcoated (right) (adapted from (Santoliquido et al., 2021), under the Creative Common CC BY license) (II): 3D printed complex hollow structure (adapted from (Chen et al., 2019) with permission (© 2019 Elsevier Ltd. and Techna Group S. r.l.)) (III) honeycomb and twisted honeycomb as-printed structures (adapted from (Zakeri et al., 2021) under the Creative Commons Attribution 4.0 International (CC BY 4.0)).

durability during thermal cycling. On the contrary, the use of SL allows the fabrication of monolithic SOFC stack in a single step. In this work, first a solid 3-tubes YSZ electrolyte was printed, debinded at 600 °C under vacuum and sintered at 1,550 °C in air. Then the oxide fuel cell stack was obtained through the deposition of cathode and anode electrodes on the outer and inner surface of the electrolyte tubes, respectively, followed by sintering at 1,050 °C for 2 h. The success of the innovative process was proved through the electrochemical characterization that showed better performance (in terms of power density) of the 3D printed stack compared to the honeycomb configuration prepared by conventional extrusion methods. In Figure 10, a comparison between the traditional multi-step stack preparation and the innovative single-step 3D printing is displayed: the simplified process, with less manufacturing stages, allows to decrease initial investment and production costs, which is considered one of the main barriers for the market up-take of the SOFC technology (Masciandaro et al., 2019).

Despite increasing interest in the use of alternative fuels, as well explained in the previous paragraph, conventional diesel or gasoline powered vehicles are still dominant. Therefore, a still important research field is dedicated to the removal of the pollutants generated by those engines. Catalytic converters (CCs) represent the state-of-the-art technology in the automotive industry to eliminate or reduce toxic emissions (Zakeri et al., 2021). These devices are able to implement the catalytic conversion of selected pollutants, including carbon monoxide, hydrocarbons, and nitrogen oxides, into less toxic or even inert products, such as CO_2, H_2O and N_2. CCs typically consist of i) a substrate (a metal or ceramic with a honeycomb structure), ii) a washcoat layer, and iii) an active catalyst (often a mix of precious metals) (Zakeri et al., 2021). The substrate, while supporting the catalyst, should satisfy some main requirements: high physical, chemical and thermal stability and low thermal expansion coefficient, to resist cracking and thermal shock due to the quick temperature variations during driving. However, as the surface area of the substrate is typically low, limiting the extension of the catalysts on its surface, an intermediate high surface area layer is interposed, named washcoat. This thin layer (10–150 µm) made by a porous ceramic material is placed on the inner walls of the substrate, and provides a wide area for dispersion of the catalyst, which is finally added to the structure by impregnation. The pollutants diffuse within the waschoat and react on the active catalyst sites.

With reference to the ceramic substrate, honeycomb-shaped cordierite is the current benchmark. The structure is obtained by extrusion, which provides regular and closed (i.e., not communicating) channels, named cells. This system, however, is characterized by a low heat and mass transfer, due to the laminar flow of the gases passing through their straight channels. A solution if offered by open cells structures, characterized by inner tortuous paths that enhance gas-wall interactions and contribute to lower thermal inertia, while providing higher conversion efficiencies (Lucci et al., 2015; Papetti et al., 2018). In this frame, ceramic 3D printing technologies offer completely new possibilities to design and develop customized architectures, aimed at maximizing geometric surface area and improving mass and heat transfer (Lucci et al., 2015).

With this goal, Papetti and co-workers (Papetti et al., 2018) designed new open cell polyhedral lattice structures, to be used as the

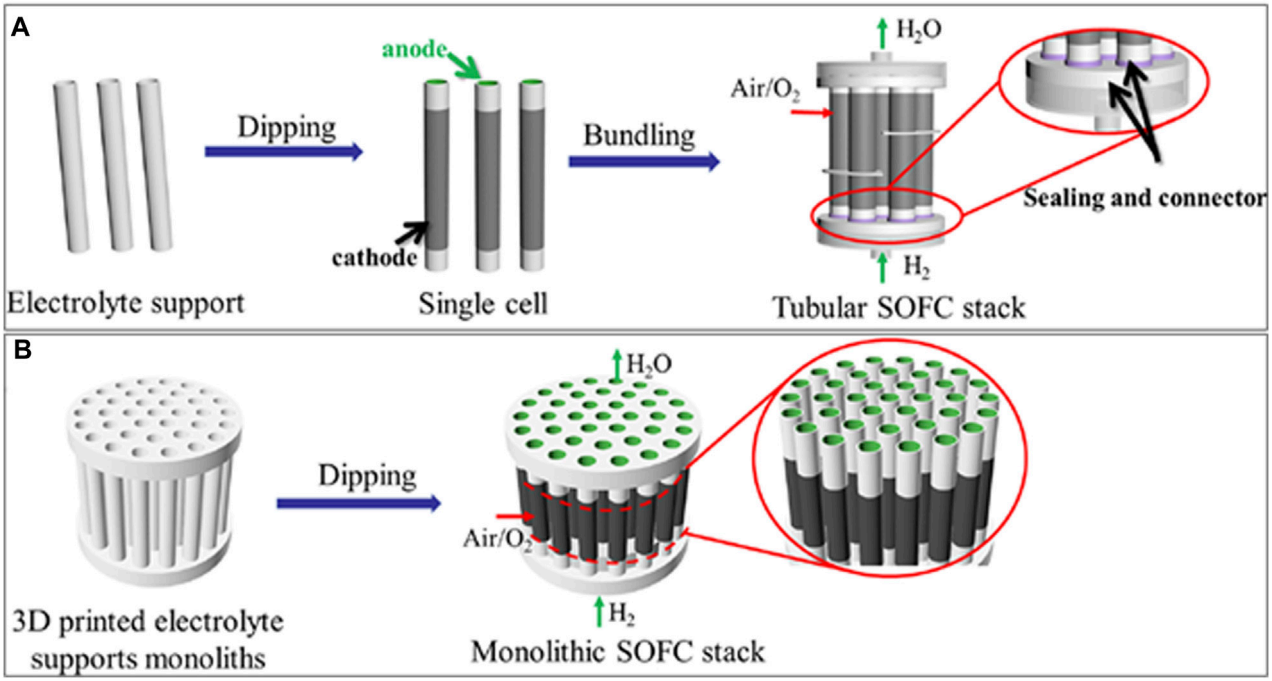

FIGURE 10
SOFC stack prepared by **(A)** traditional multi-step manufacturing process and **(B)** SL. Image adapted from (Jia et al., 2022) with permission (© 2022 Elsevier Ltd.).

substrate in CCs, as an alternative to the traditional honeycomb configuration. Different architectures have been designed, and the optimal one (in terms of shape and dimension) was selected on the ground of numerical simulations based on mass transfer and flow resistance. These architectures were based on cubic, kelvin and octet truss elemental cells, where the cubic cell was designed with two different orientations, parallel and rotated by 45°, meaning that the spatial diagonal of the cube was aligned to the main gas flow. All the open cell polyhedral structures showed higher mass transfer coefficients than the honeycomb one and the best result was found for the 45°-rotated cubic cell. The selected cubic structure was subsequently 3D printed by SL, by using an Al_2O_3-based resin. After sintering, the washcoat layer was obtained by dip coating into a Pt-γ-Al_2O_3 suspension, followed by a calcination at 600 °C. Experimental measurements were carried out in a model gas reactor, determining the conversion (oxidation) of C_3H_6 hydrocarbons. The test confirmed the mass transfer advantages of the polyhedral structures as predicted by the simulations: in fact, the rotated cube and honeycomb structure achieved the same conversion, which was a successful result considering the much lower surface area of the cubic architecture.

Based on these results, Santoliquido and co-workers (Santoliquido et al., 2021) developed by SL the same rotated cubic cell structure (Figure 9B, top image) for the catalytic conversion of NO into NH_3. For this purpose, the 3D printed Al_2O_3 cell, after sintering, was coated by a layer composed by V_2O_5-WO_3-TiO_2. Similarly, to the previous work, results showed that the wetted surface area of the 3D-printed lattice was about half that of a traditional honeycomb, to get similar conversion, meaning less catalyst to get the same conversion activity.

Still with the aim to provide innovation to the support for CC, Chen and co-workers (Chen et al., 2019) developed by DLP a cordierite structure, with a highly complex architecture, characterized by perpendicularly intersecting hollow structure with a skeleton thickness being as small as 300 μm (Figure 9B, bottom left image). To achieve this result, efforts have been dedicated to the elaboration of a suitable resin and to the optimization of the printing parameters. The optimal formulation was designed by investigating the role of the cordierite particle size, solid content and dispersant amount on the rheological behaviour as well as on ceramic resin sedimentation tests. The photocurable resin formulated by 40 vol% solid content, 0.35 μm particle size and 5 wt% dispersant concentration showed the best stability and flowability. The effect of the photoinitiator on the penetration depth was investigated as well, showing that he addition of 2 wt% photoinitiator generated an optimal curing process, and allowed the thickest curing depth for the optimal formulation.

An innovative contribution in the field of 3D printed CCs was provided by Zakeri and co-workers (Zakeri et al., 2021), where a self-supporting structure made of a washcoat materials was fabricated by SL (Figure 9B, bottom left image), reducing the manufacturing time and simplifying the whole process. To this aim, a photocurable formulation containing γ-Al_2O_3 and CeO_2 (a commonly used washcoat materials in CCs) was shaped into honeycomb and twisted honeycomb structures. A key issue in the process was related to the presence of CeO_2 that significantly reduced the penetration depth of the UV light, due to absorbance phenomena. As a further challenge, the sintering temperature had to be optimized by keeping into consideration two opposite trends: while a low-temperature sintering (such as 900 °C) was

necessary to prevent the phase transformation of the γ-Al_2O_3 into the α-phase (that causes the reduction of the specific surface area), a higher temperature (1,100 °C) would be beneficial for the mechanical strength. This duality was not solved by the authors, who deserved to further studied the sintering of the 3D printed parts.

Still in the energy and environmental fields, there is a growing interest towards piezo-electric ceramics characterized by complex structures, being this aspect almost completely unexplored due to the very limited success of the conventional manufacturing processes to develop non-conventional architectures. The applications of piezo-ceramics are wide, and range from energy harvesting to acoustic imaging for the biomedical sector. First attempts to obtain complex structures by vat-photopolymerization techniques are provided in the following.

Liu and co-workers (Liu et al., 2021a) developed a barium titanate ($BaTiO_3$) resin for DLP, highlighting the challenge in the printing process due to the high scattering induced by the refractive index (RI) mismatch between the liquid monomer and the ceramic particles. In order to overcome this issue, different monomers, having different RI, were tested. Results based on measuring the curing depth of irradiated slurries allowed to select the best monomer (acryloyl morpholine). After optimizing the solid loading, complex-structured $BaTiO_3$ parts were successfully fabricated and sintered, achieving high density (95.3%). After the dielectric and ferroelectric properties of the sintered material were characterized, a hydrophone prototype was developed, proving the feasibility of DLP in the manufacture of complex-structured ceramics and functional devices.

Chen and co-workers (Chen et al., 2016b) developed a $BaTiO_3$ resin and used a Mask-Image-Projection-based SL (MIP-SL) to fabricate ultrasonic sensing devices. First attempts were performed on 3D printed cylinders, which were characterized by proper piezoelectric constant and relative permittivity. Then, complex parts were fabricated, and, namely,: *i*) a segment annular array (3D-SSA), containing 64 pillars characterized by fan shape (while, traditionally they are shaped in square or rectangular shape), and *ii*) a concaved-shape piezoelectric element (CPE) to be tested in an ultrasonic transducer. In Figure 11, the design a) and the 3D printed parts d) are displayed. The pulse and echo signal showed that the 3D printed parts were able to convert compressive/tensile stress to electric charge, and *vice versa*.

In the frame of sensing ceramics, some attempts to develop 3D printed complex devices as gas sensors have been performed. Zhou and co-workers (Zhou et al., 2020) developed a 3D body-cantered periodical mullite structure, to be used as a substrate for ammonia sensing devices. A commercial mullite resin was employed in a DLP equipment, and the 3D printed parts were sintered at 1,500 °C for 4 h. The ceramic substrates were then decorated with polyaniline (PANI) and Ag ions, acting as the sensing layers. The sensor exhibited proper response towards ammonia a very good selectivity towards other gases, with superior mechanical properties compared with conventional devices. The same research group (Zhou et al., 2022) further developed, still using DLP, a SiOC based ammonia sensor, with a honeycomb structure made by micro-tunnel, which was designed to provide both load-bearing and self-protecting characteristics. The ceramic substrate was then decorated with polypyrrole and TiO_2 particles, acting as ammonia sensing layer. Room-temperature selectivity and long-term stability were successfully achieved in this device.

In the environmental field, the use of 3D printing in the engineering and development of membranes and filters for water purification deserves to be mentioned.

Chevarin and co-workers (Chevarin et al., 2023) designed micropatterned Al_2O_3 membranes, as an anti-fouling strategy. In fact, the cleaning of the membranes by the fouling requires periodical interruption of the filtration process, which prolongs operative times and reduces membrane durability. The design of proper inner architectures can promote turbulence in the flow and reduce fouling deposition. The research was supported by computational fluid dynamics simulation, which allowed to optimize the geometry of the membrane inner surface, in term of inter-ring distance (from 2 to 5 mm) and ring profile (symmetric or asymmetric). Once defined the best architecture, membranes were printed by SL, and sintered at 1,200 °C. Microfiltration tests were carried out on both smooth and patterned membranes, by using bacteria aqueous solutions, showing a significant role of the inner rings in reducing cake formation, especially at high crossflow velocity.

Chen and co-workers (Chen et al., 2019) developed 3D printed Al_2O_3 substrates to be used in water/oil separation technology. The porous structures, after sintering, were coated with *in situ* growth aluminium borate superhydrophilic whiskers, thus to play and opposite role when in contact with water and oil. The versatility of the DLP in building different structures, was here fully exploited. The authors, in fact, demonstrated that the design of the 3D printed parts needs to be optimized according to the specific applications. Thus, meshes, foams, and scaffolds, were fabricated for oil/water mixture separation, oil purification from water and emulsion separation, respectively.

4.1 Ceramic SL and DLP in energy and environmental field: relevant outcomes and final considerations

All the presented works demonstrated the tremendous potential of ceramic 3D printing in the energy and environmental fields. However, several issues still need to be faced, and many steps taken to bring the technology to more mature levels, towards its industrialization. In particular.

- The ability of tuning the inner architecture of cells and membranes can be seen as a revolution in the energy sector. In fact, the possibility to increase and modulate the specific surface area and thus the performance of devices operating in different types of applications (SOFCs, catalytic converters, sensing ceramics and water filtration systems) is an unprecedented advantage;
- The very high resolution can be exploited for the fabrication of smaller and smaller objects, towards the miniaturization of energy devices;
- Few but relevant examples showed that AM technologies allows to decrease the number of manufacturing steps of certain devices (like SOFC stucks), saving time and money. The impact of 3D printing on the productivity and durability of devices is well demonstrated by the fabrication of patterned

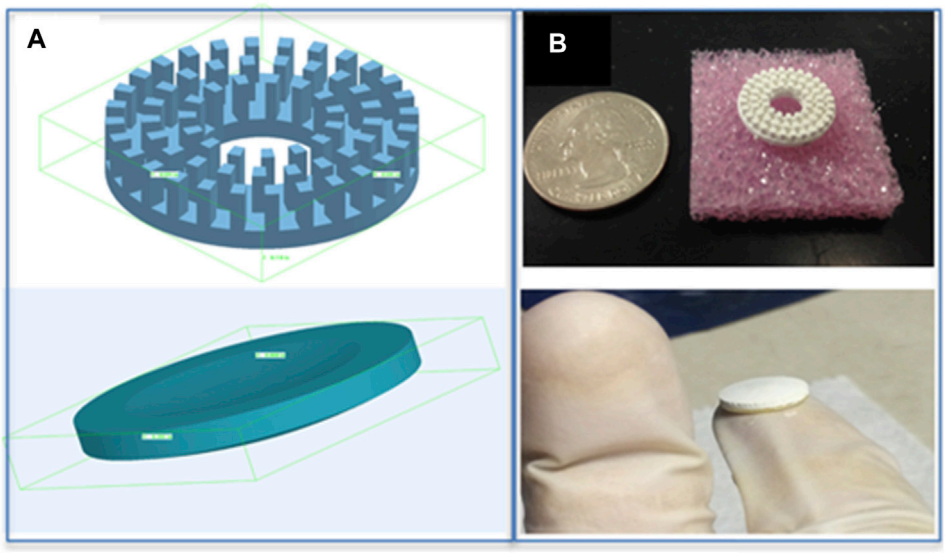

FIGURE 11
Design **(A)** and 3D printed **(B)** parts: the annular array with the 64 pillars (top) and the concaved-shape piezoelectric element (bottom). Image adapted from (Chen et al., 2016b) with permission (© 2016 Elsevier Ltd.).

water filtration membranes, designed to reduce inner fouling and consequently to avoid interruption of the filtration process;
- Most of the described electrochemical, energy and environmental devices are multi-material/multi-ceramic components. Thus, the most important unmet challenge today is the difficulty of implementing multi-material capabilities in the current vat-photopolymerization equipment.

5 Space and aerospace applications

Different classes of advanced ceramics find application in space and aerospace industry, including both oxide- and non-oxide ceramics and ceramic composites. This is mainly due to their exceptional dimensional/chemical stability over a wide temperature range and high corrosion resistance, as well as a lower density compared to metal-based components, which is fundamental in achieving faster speeds with lower fuel consumption. Furthermore, advanced ceramics can be used for the manufacturing of piezoelectric, thermoelectric and electrochemical sensing devices (Shapiro et al., 2016), with potential applications in the space industry.

Over the last decades, AM processes have successfully established themselves in aerospace fields for the production of prototypes, rapid tooling and repair and Direct Digital Manufacturing of metal, polymeric, ceramic and composite materials (Kumar and Krishnadas Nair, 2017; Najmon et al., 2019; Martinez et al., 2022a; Karkun and Dharmalinga, 2022). However, compared to metal processing, the application of AM to ceramics for space and aerospace is still quite immature at both research and industrial levels, owing to multiple technological challenges intrinsic in ceramic processing.

Despite this, vat-photopolymerization-based strategies find practical application in the production of ceramic cores and shells for investment casting of nickel superalloys, actively entering the production cycle of hollow turbine blades for aircrafts engines. These components are characterized by a complex design, fine-tuned to maximize engine performances in terms of thrust, fuel and overall efficiency by the presence of cooling channel and holes to withstand very high temperatures. A comprehensive picture of ceramic molds for investment casting has been recently provided in a review paper by Kanyo and co-workers (Kanyo et al., 2020) who discussed multiple aspects related to the design, processing and testing protocols available for these components.

Compared to traditional mold-forming methods, such as gel-casting and injection molding, the use of vat-photopolymerization methods brings great advantages, as listed below (Lu et al., 2013; Kanyo et al., 2020).

1) Limited design restrictions
2) Improved dimensional and structural control
3) Possibility to tune shell thickness and permeability to preferentially address susceptible zones in the shell
4) Improved precision in layered shell components
5) Reduced production costs and material waste
6) Improved lead-time

Selection criteria for ceramic materials intended to be used within an investment casting process for making ceramic shells and cores mainly concern their reactivity, leachability, thermo-mechanical properties and processability. In particular, they should be characterized by a good phase stability at high temperature, as well as a flexural strength above 20 MPa at the casting temperature of the metal alloy. Moreover, a porosity of at least 30% is required to facilitate the chemical dissolution of the ceramic component after casting (Qin and Pan, 2009; Shabani et al., 2019).

Oxide ceramics successfully meet most of these requirements, although, in their pure form, they still present some limitations. For this reason, it is often preferable to use mixtures and composites, in order to meet as many process requirements as possible (Lu et al., 2014).

The SL process of silica-based integrally cored ceramic molds was described by several authors (Zhou et al., 2010; Bae and Halloran, 2011; An et al., 2022; Zheng et al., 2022). Among all available ceramics, in fact, fused silica is widely appreciated due to the possibility to easily tune mechanical and thermal response. In particular, at the amorphous state, it is characterized by very low thermal expansion coefficient, high thermal shock resistance and good leachability properties, although it may experience softening and thus geometric distortion during sintering.

An effective way to improve the strength of silica molds is to induce high-temperature conversion to β-cristobalite up to 10%–25%. The presence of β-cristobalite, in fact, is beneficial in structure strengthening, but higher amounts could lead to the formation of microcracking due to the volumetric contraction associated to the cubic-to-tetragonal transformation.

In these regards, Bae and co-workers (Bae and Halloran, 2011) describes the SL production of silica-based integrally cored ceramic molds, where the design of the component was optimized to shorten the production of complex hollow airfoils and maximize their performances by integrating internal cooling passages within the ceramic core.

A refractory silica powder (60 vol%) with an average particle dimension of 12 μm was added to a photocurable acrylate-based ceramic resin, reaching a curing depth of 125 μm. In order to achieve a 25% β-cristobalite fraction, the component was sintered at 1,300 °C, reaching a flexural strength of 12 MPa. However, while fine features and internal airfoil core were successfully resolved, finest trailing edge features presented a lower resolution due to the 0.125 mm focal point used in the manufacturing process. Despite this, the overall dimensional accuracy of the part was satisfactory, reporting a deviation in the XY plane from nominal dimension of approximately −0.7%, while in the *Z* direction was +0.3% for the green part, while sintering shrinkage was uniform in all the directions (Bae and Halloran, 2011).

A different approach to improve the strength of silica-based ceramic cores, still processed by SL, was reported by Zheng and co-workers (Zheng et al., 2022) who used SiC fibers as a reinforcement phase. Crystallization of fused silica, in fact, is inhibited by oxidation phenomena of SiC fibers, thus reducing linear shrinkage of silica ceramics and achieving higher dimensional accuracy. Flexural strength vs. SiC fibers content curves at room and high temperature (T = 1,550 °C) showed an increasing trend up to a maximum of 34.6 MPa corresponding to a SiC content of 4.0 wt%, thus meeting strengths requirements reported for ceramic cores for manufacturing hollow blades. However, higher SiC contents are responsible for the rapid conversion to β-cristobalite associated to the propagation of microcracking and determining a significant drop in mechanical properties. Therefore, the optimum addition of SiC fibers below 4 wt % can provide silica-based ceramic cores with excellent mechanical properties, which promote application and development of silica ceramic cores for the manufacturing of hollow blades.

Main challenges related to the production of silica-based SL 3D printed ceramic cores for hollow aeroengine turbine blades were meticulously addressed by An and co-workers (An et al., 2022). This scientific contribution is worthy of attention due to the systematic approach followed in all the manufacturing/characterization stages, until the metal component was fully and successfully realized. High solid loading ceramic slurries based on fused silica with 2vol% ZrO_2 with excellent rheology and good photopolymerization behavior were produced to print ceramic core samples ($40 \times 10 \times 4$ mm^3) using DLP. The effect of process parameters on microstructural evolution, cracking, bending strength, shrinkage and porosity were analyzed, allowing to define an operative approach to the evaluation and prediction of the above parameters. Basing on statistical analysis of the performance data of the ceramic cores, detailed Ashby charts were obtained to support the overall design/production process of these components up to their final use.

Al_2O_3 has also been extensively studied as suitable material for core/shell fabrication. Compared to fused silica ceramics, Al_2O_3 exhibits a better chemical stability at high temperature and creep resistance. Additional advantages are related to the possibility of ease leachability by aqueous HF or KOH solutions, as well as high thermal conductivity and suitable thermal expansion coefficient (Kanyo et al., 2020). Moreover, Al_2O_3 ceramics leachability could be further improved by the addition of pore forming agents and easy-to-corrode phases (e.g., $CaCO_3$, SiO_2, β-Al_2O_3) (Zhu et al., 2019).

Shrinkage behavior, mechanical and microstructural properties of Al_2O_3-based ceramic cores have been object of study of different research groups (Li et al., 2020b; Li et al., 2022a; Li et al., 2022c; Gu et al., 2023). According to Li and coworkers (Li et al., 2022a), the mechanism of crack growth and propagation within Al_2O_3 ceramic cores obtained by DLP and subjected to flexural mechanical testing is strongly dependent on the sintering temperature. In particular, sintering temperature below 1,400 °C induced a crack propagation along the Al_2O_3 grain boundaries by an intergranular mechanism, reaching a flexural strength of 20.3 MPa. However, by increasing the sintering temperature up to 1,550 °C, cracks propagated according to an intragranular mechanism, determining an increase in flexural strength.

Sintering atmosphere could significantly improve final properties of Al_2O_3 ceramic cores without inducing any changes in phase composition and chemical bond structure. In particular, vacuum sintering was found to be more efficient, allowing to reach significantly higher flexural strength (33.7 MPa) at lower temperatures (1,150 °C), yielding a ceramic component with bulk density of 2.43 g/cm^3, open porosity of 37.9% and linear shrinkage of 2.3%, 2.4%, and 5.3% in the X, Y, and Z directions, respectively.

In these regards, finding effective ways to mitigate material shrinkage upon sintering is of paramount importance in the production of ceramic molds for aerospace industry to preserve geometrical fidelity. As already mentioned, increasing the solid loading within photocurable ceramic resin actively contributes in reducing volumetric shrinkage, but dramatically decreases curing depth and printing quality due to scattering phenomena.

Some studies by-pass this issue by proposing alternative strategies based on the use of additives within the ceramic resin. As an example, SiO_2 was found to be effective in improving the performances of Al_2O_3 ceramic cores, reducing sintering shrinkage and mitigating the excessive strength of the component.

In these regards, Li and co-workers (Li et al., 2022c) described a new approach based on an *in situ* mullite synthesis, based on the thermal reactivity between Al_2O_3 and SiO_2, leading to the formation of a mullite phase. In particular, DLP was used to process high solid loading (55 vol %) photocurable ceramic suspensions based on Al_2O_3 and variable SiO_2

amounts (up to 25 wt%). Minimum shrinkage was obtained for a fused silica content of 20 wt%. The study revealed the possibility to optimize the properties of Al_2O_3 ceramic core by properly combining silica content and processing parameters. In particular, high open porosity (40 vol%), suitable high-temperature bending strength (25 MPa, 1,500 °C) and low shrinkage along the *z*-axis were found for samples sintered at 1,400 °C with a fused silica content of 20 wt%.

Other issues to be addressed are related to the casting of metal alloys and the interaction of the melt with the ceramic shells used in investment casting. Due to the high temperatures involved in the process, in fact, low thermal expansion coefficients ceramics have to be preferred in order to prevent both dimensional defects and residual stresses in the casting resulting from the geometrical distortion of the component. According to this, having the ability to directly predict and control the thermal expansion of a material would certainly represent a quantum leap in the production of high temperature precision devices, where shape accuracy under large-span temperature ranges is strongly required.

In this regard, SL-based manufacturing process of Al_2O and ZrO_2-based multi-ceramic structures with tunable thermal expansion has been recently described by Zhang and co-workers (Zhang K. et al., 2021). In particular, structures with positive, zero and negative thermal expansion coefficients were obtained starting from Al_2O_3 and ZrO_2 ceramics with positive thermal expansion. Structural design was optimized on the basis of dual-ceramic triangle structure, with the bottom and the hypothenuse made of two different ceramic materials characterized by different thermal expansion behavior. Thermal mismatch was successfully managed by mean of functionally graded ceramic layers, creating a heterogeneous material able to efficiently release thermal mismatch stresses.

Finally, Schwarzer-Fischer and co-workers (Schwarzer-Fischer et al., 2022), developed Al_2O_3-based photocurable ceramic resins for the production of cold-gas satellite thrusters with 2.5 N and 10 N thrust (Figure 12). Authors highlighted the influence of the monomers on the flow behavior during printing process as well as the importance of resin formulation for an efficient and optimal debinding phase, resulting in a measured density above 99% of the theoretical density.

Last decades have marked by great scientific fervor around the application of silicon carbide (SiC) ceramics in aerospace industry (Lamicq, 1999). Such a technological interest is strongly justified by a winning combination of high strength, high temperature chemical stability, high thermal conductivity and strong wear resistance. However, additional challenges arise from the need to combine light absorbing and high RI materials with vat-photopolymerization techniques.

For this reason, most of the available literature studies focus on the optimization of photocurable behavior of SiC-based resins by carrying out systematic studies addressing the influence on the printability of SiC components of different parameters, such as resin monomers, dispersant, particle size, solid loading, ball milling time and use of fillers (Ding et al., 2020a; Tang et al., 2021).

SiC materials show a great potential for the production of space-based lightweight optical mirrors. Ding and co-workers (Ding et al., 2020b) reported the production of lightweight SiC ceramic optical mirror by SL. Commercial micron-sized SiC with an average particle size of 15 μm and nanosized SiC with an average particle size of 40 nm were used as basic materials, while Al_2O_3 and Y_2O_3 powders were used as sintering additives. The overall manufacturing process included polymer burn-out, pre-sintering and precursor infiltration and pyrolysis to improve the relative density and the flexural strength of the final product up to 93.5% and 165.2 MPa, respectively. However, additional efforts should be performed to increase the dimension of the component, definitely too small for the intended application.

Space and aerospace industry and additive manufacturing technologies have always represented innovation and progress in the collective imagination. Perhaps this is precisely why it is difficult to confine 3D printing to terrestrial applications. Rapid prototyping and 3D printing technologies have already shown their potential in space manufacturing, helping in finding practical solutions to logistic problems for long-duration human spaceflight and colonization of alien stars. To this extent, Dou and co-workers (Dou et al., 2022) investigated the optimisation of ceramic pastes for SL in microgravity environments. This was possible thanks to an accurate control over the rheological properties of ceramic pastes by adding HE-cellulose or carbomer 940 as thickening agents, conferring a Bingham pseudoplastic behavior properly tuned for possible use under 0 gravity, Mars gravity and Moon gravity, with limited wall climbing phenomena. The work supported the concrete possibility to use additive manufacturing in space, pushing research beyond its current limits with the aim of extending extraterrestrial additive manufacturing to new materials such as lunar regolith (Altun et al., 2021; Isachenkov et al., 2021). Based on this, it seems fitting to conclude the present section by mentioning a very recent study by Aguiar and co-workers (Aguiar et al., 2023) that investigated the possibility to use Greenland Anorthosite (a lunar regolith simulant containing Al_2O_3, SiO_2, and Al_2SiO_5 as major phases) for 3D printing using DLP. The aim was to use locally available lunar materials for the *in situ* structures construction (including an igloo) to be developed in the future Moon colonization (Figure 13).

5.1 Ceramic SL and DLP in space and aerospace field: relevant outcomes and final considerations

In relation to the two application areas illustrated in the previous sections, namely, biomedical and energy/environmental, it is evident that in the space/aerospace sector, AM technologies for ceramic processing are still confined to a few well-established applications. However, relevant considerations can be made.

- The advantages deriving from the application of vat-photopolymerization are gradually leading to the overcoming of traditional core and shell manufacturing techniques based on the use of expensive and time-consuming molds.
- As in the case of dental prostheses, optimal control over the geometric characteristics of the part is required in order to achieve accurate reproduction of the complex geometries involved in the design of turbine blades to maximize the performance of aircraft engines.
- In addition, the use of these components for high-temperature investment casting of metal alloys makes it essential to deepen our knowledge of the thermal expansion of materials, finding innovative engineering solutions aimed at obtaining materials with a minimum expansion coefficient.

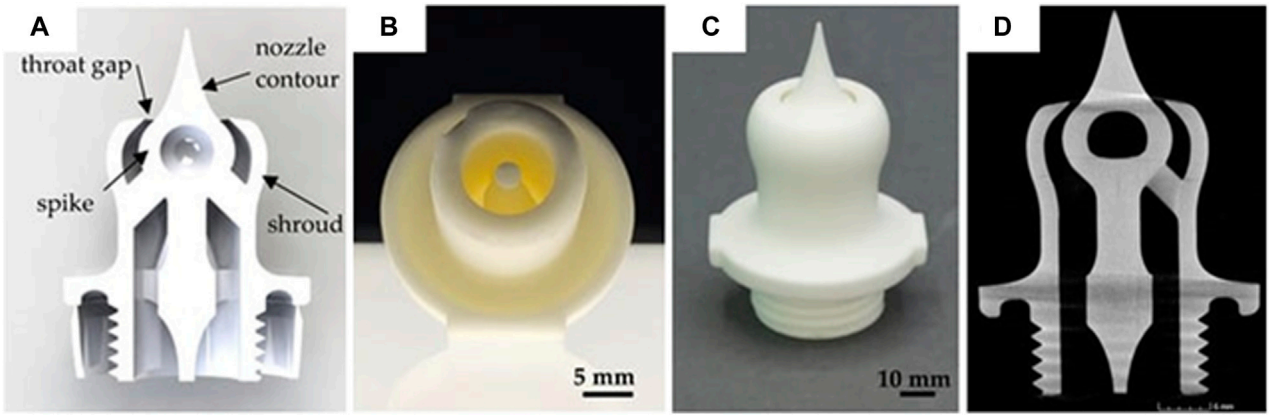

FIGURE 12
Al_2O_3 nozzles additively manufactured using the CeraFab 7,500 printing device (Lithoz, 2023). Sectional view of an aerospike nozzle **(A)**; 2.5 N nozzle **(B)**, 10 N nozzle **(C)** and CT image of the 10 N nozzle **(D)**. Image adapted from (Schwarzer-Fischer et al., 2022) under the Creative Commons Attribution CC BY License.

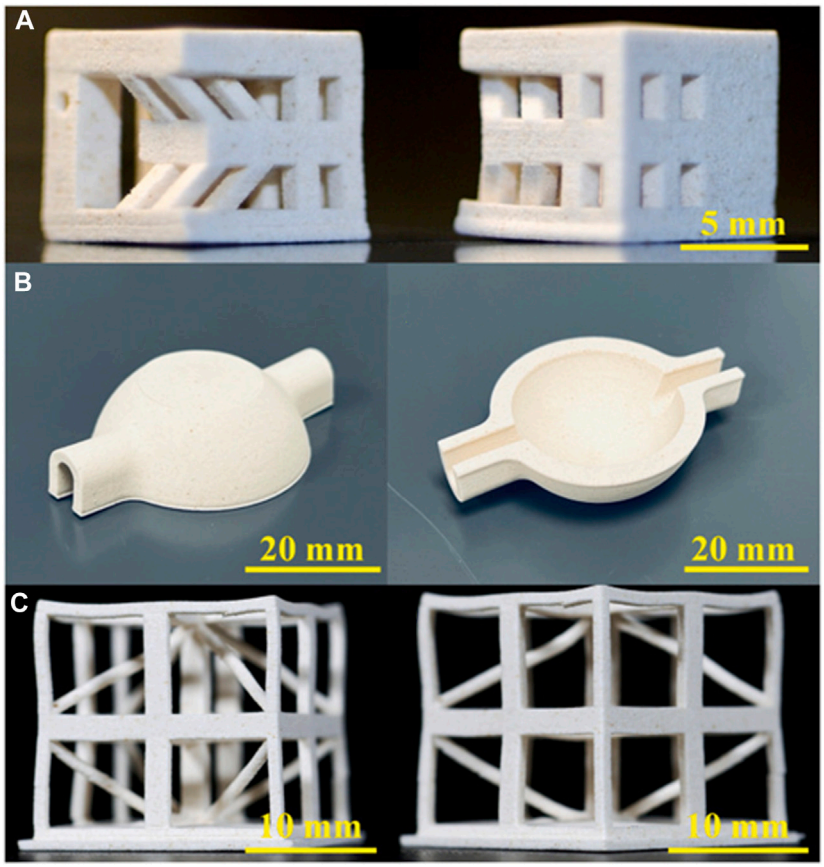

FIGURE 13
Greenland Anorthosite lunar regolith-based components fabricated by DLP. Image reproduced with permission from (Aguiar et al., 2023) (© 2023 Elsevier Ltd. and Techna Group S. r.l.).

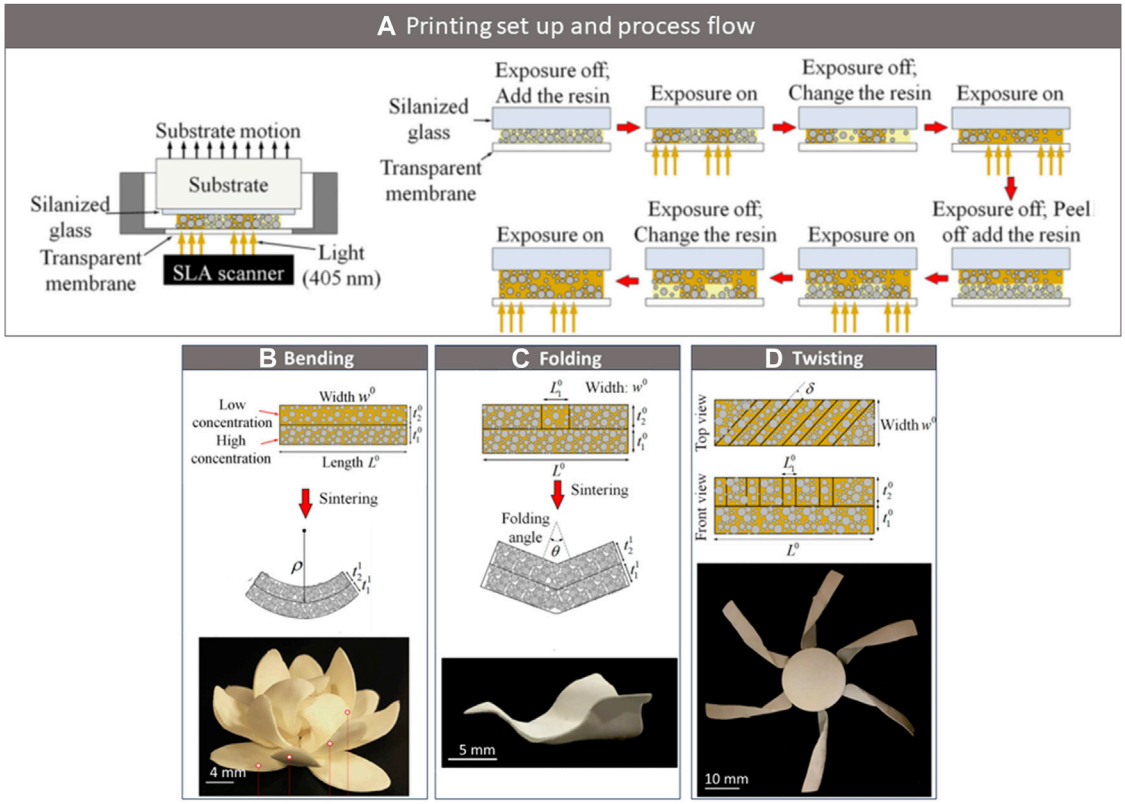

FIGURE 14
Rationally design self-shaping ceramics: **(A)** printing set up and process flow; **(B)** bending, **(C)** folding and **(D)** twisting mechanism in Al_2O_3 components with tailored anisotropic behavior upon sintering. Image adapted from (Ding et al., 2022) with permission (© The Royal Society of Chemistry 2022).

6 Vat-photopolymerization of ceramics: what is expected in the coming years

3D printing has represented a great revolution in the field of materials shaping, allowing to overcome major issues and drawbacks of traditional ceramic processing in different application fields. Between limitations and new opportunities, vat-photopolymerization is continuing to inspire the scientific community to the discovery of its full potential.

Certainly, multi-material printing fits into this framework. Through this process it is in fact possible to obtain objects exhibiting heterogeneous characteristics (Chen et al., 2022a; Shaukat et al., 2022a), such as different colors, electrical conductivity, insulation and mechanical properties, partly addressed in the previous sections.

Although the trend is definitely on the rise, multi-material printing of ceramics still presents relevant technological challenges that will certainly play a leading role in the years to come. Apart from proposing valuable strategies to avoid cross-contamination and time-consuming cleaning procedures, new protocols specific to ceramic material coupling need to be defined, in order to prevent the formation of cracks, pores and residual stresses, detrimental for the integrity of the components, the dimensional stability, crack growth resistance and mechanical properties exercise. In these regards, optimisation of co-debinding and co-sintering processes cannot be achieved without a careful selection of raw materials basing on their chemical compatibility, in order to favor the formation of atomic bonds. Another key aspect to be considered is the mismatch in terms of thermal properties, i.e., thermal expansion coefficient, while volumetric shrinkage will be appropriately modulated by slurry formulation, guaranteeing the minimum printability requirements detailed above.

Despite this, few successful preliminary studies are already reported in literature, showing promising results (Xing et al., 2020b; Zhang et al., 2021b; Hu et al., 2022) and leading companies in the field have launched their own range of 3D printers based on photopolymerization technology dedicated to multi-material printing (Lithoz, 2023 and Admatech, 2022).

In recent years, interesting studies have appeared in the literature regarding the creation of tailored composition gradients within the part to induce specific shape changes upon firing (Ding et al., 2022). These materials are known as rationally-designed self-shaped ceramics. The printing set up and the process flow are depicted in Figure 14A. Compared to other additive manufacturing technologies, vat-photopolymerization printing strategies allow to efficiently manage particles concentration variation within the 3D object at high resolution, resulting in an accurate control over bending (Figure 14B), twisting (Figure 14C), or folding (Figure 14D) mechanisms upon thermal treatments.

In addition, dedicated length scale and material-independent model have been developed to univocally predict experimental shape changes (Ding et al., 2022).

However, as for multimaterial printing, time consuming cleaning procedures are required to switch from high-to-low concentration slurries.

This approach certainly represents a breakthrough in the shaping of ceramic materials with complex geometries, allowing through the simple printing of bi-layer components to achieve complex geometries by exploiting anisotropic shrinkage, making the technique appealing in the production of components for a variety of applications such as hermetic sealing of electronics, protective systems, architectural design and construction, molds for fabrication of gas turbines, hydraulic valves, and wire guides in textile manufacturing.

In a broader sense, the possibility of obtaining geometrically complex components in a controlled manner can be considered the dawn or transition from 3D manufacturing techniques to 4D printing, i.e., the realization by 3D printed "smart" objects capable of autonomously modifying their shape and properties to exert a specific function in response to an external stimulus of a physical, chemical or biological nature.

An example of smart materials for the production of printed 4D components is certainly piezoelectric ceramics, finding applications not only in energy and environmental field but also in bone tissue engineering, as smart material for the production of biomimetic scaffolds reproducing the physiological electrical microenvironment. Among piezoelectric ceramics with potential use in bone repair, hydroxyapatite and KNN-based caramics ($K_{0.5}$-$Na_{0.5}$-NbO_3) are attracting the attention of the scientific community due to their exceptional piezoelectric response and mechanical behavior matching that of native bone tissue (Chen et al., 2023).

Although publications on 4D printing are clearly on the rise compared to previous years, these are in most cases preliminary studies in the development phase. With specific reference to vat-photopolymerization, very few studies have been reported, most of them in the biomedical and environmental/energy fields, while research related to space and aerospace applications mainly rely on the use of other printing technologies, such as direct ink writing, which has been significantly more explored (Liu et al., 2018; Li et al., 2022d; Wang et al., 2023a).

In this sense, it is clear that 4D printing of ceramic materials based on vat-photopolymerization technology is clearly lagging behind other additive technologies, such as extrusion techniques. This can be attributed to several factors, such as the difficulty of finding smart ceramic resins suitable for the printing process and ceramic precursors prone to deformation, as well as the high brittleness of ceramic materials, which certainly lend themselves less to externally induced shape changes. For this reason, a large part of the research activities in this field concern 4D-printing ceramic-reinforced polymer matrix composites (which are, however, out of the scope of this review), which have already shown great potential in the energy/environmental fields as gas adsorption devices (Zhang et al., 2022b).

An interesting challenge for the future could concern the optimization of light-curing resins based on polymeric ceramic precursors, showing easier processability, flexible designability, and relatively low sintering temperature. This approach has already been successfully used in combination with extrusion techniques for the production of lightweight self-shaping ceramics for sensing and actuation applications and elastomer-derived ceramic structures for aerospace propulsion components, space exploration and bio-inspired tough ceramic/organic hybrid materials (Liu et al., 2018).

In conclusion, multi-material 3D/4D printing has definitely the potentialities to improve the quality of AM ceramic components, paving the way for new advanced applications through cutting-edge approaches, not easily accessible through conventional techniques.

7 Conclusion

The present review opens a window to the world of vat-photopolymerization technologies applied to ceramic materials, providing a transversal analysis of the state-of-the-art of SL and DLP in relevant technological industrial/research fields of our times, including biomedicine, energy, environment and space/aerospace, with the aim of highlighting the potential, critical issues and open challenges for the technology transfer on industrial scale.

Literature survey revealed major achievements in the biomedical sector, where the possibility of producing highly defined and patient-specific devices fits well with the needs of the medical field. A clear example of this is represented by TPMS structures, still poorly used in energy/environmental sector, but highly valued as scaffolds for tissue engineering in support of cell colonization and migration and nutrient transport.

Functionally-graded scaffolds represent one of the greatest promises for the future, allowing the production of multi-functional structures with gradient properties suitable for interfacial tissue engineering. Similar approaches could be adopted in devices operating in other sectors, like CCs, sensing and filtration systems, where high mechanical strength has to be conjugated with a highly porous, functional structure.

In energy and environmental applications, multi-material printing still remains the main unmet challenge.

Compared with the multi-material additive manufacturing of liquid photocurable resins used in the biomedical sector, multi-material vat-photopolymerization of ceramic resins is more and more challenging due to the higher viscosities involved and risk of cross-contamination. However, few successful preliminary studies are available, presenting encouraging results.

In addition, in almost all the investigated sectors, numerical simulations resulted to be a very useful tool to select among the uncountable new designs allowed by 3D printing the most suitable for certain applications. Closer and closer collaborations among computation and experimental methods seems the key to success for the further advancement of the 3D printing of ceramics.

The tremendous potential of SL and DLP applied to ceramic materials is fully demonstrated in this review, as claimed in most of the cited literature reporting enthusiastic and highly promising experimental results.

This has determined, among the other things, a significant resonance at the industrial level, pushing R&D departments of leading companies working on ceramic SL and DLP to produce and distribute commercial ceramic resins to be used in energy, medical and space/aerospace fields. In spite of this, a further widening of the portfolio of available ceramic resins is desirable, as it will boost research and its translation to prototyping, towards the industrialization and market-uptake of the technology and related products.

Author contributions

Conceptualization, EF, PP; Investigation, EF, PP; Methodology, EF, PP; Supervision, PP, BC, LM; Validation, EF, PP, and BC; Writing—original draft, EF, PP, and BC. All authors contributed to the article and approved the submitted version.

Funding

This publication is part of the project NODES which has received funding from the MUR – M4C2 1.5 of PNRR funded by the European Union - NextGenerationEU (Grant agreement no. ECS00000036).

Conflict of interest

The authors declare that the research was conducted in the absence of any commercial or financial relationships that could be construed as a potential conflict of interest.

Publisher's note

All claims expressed in this article are solely those of the authors and do not necessarily represent those of their affiliated organizations, or those of the publisher, the editors and the reviewers. Any product that may be evaluated in this article, or claim that may be made by its manufacturer, is not guaranteed or endorsed by the publisher.

References

Admaflex 300 multi-material-combined multi-material and High volume mono-material (2022). Available at: https://admateceurope.com/admaflex300-multimaterial (Last access September 26 2023).

Aguiar, B. A., Nisar, A., Thomas, T., Zhang, C., and Agarwal, A. (2023). *In-situ* resource utilization of lunar highlands regolith via additive manufacturing using digital light processing. *Ceram. Int.* 49, 17283–17295. doi:10.1016/j.ceramint.2023.02.095

Ahamed, M. K., Wang, H., and Hazell, P. J. (2022). From biology to biomimicry: using nature to build better structures – a review. *Constr. Build. Mater* 320, 126195. doi:10.1016/j.conbuildmat.2021.126195

Al-Ketan, O., and Abu Al-Rub, R. K. (2019). Multifunctional mechanical metamaterials based on triply periodic minimal surface lattices. *Adv. Eng. Mater* 21, 1900524. doi:10.1002/adem.201900524

Al-Ketan, O., Pelanconi, M., Ortona, A., and Abu Al-Rub, R. K. (2019). Additive manufacturing of architected catalytic ceramic substrates based on triply periodic minimal surfaces. *J. Am. Ceram. Soc.* 102, 6176–6193. doi:10.1111/jace.16474

Ali, D., Ozalp, M., Blanquer, S. B. G., and Onel, S. (2020). Permeability and fluid flow-induced wall shear stress in bone scaffolds with TPMS and lattice architectures: A CFD analysis. *Eur. J. Mech. - B/Fluids* 79, 376–385. doi:10.1016/j.euromechflu.2019.09.015

Altun, A. A., Ertl, F., Marechal, M., Makaya, A., Sgambati, A., and Schwentenwein, M. (2021). Additive manufacturing of lunar regolith structures. *Open Ceram.* 5, 100058. doi:10.1016/j.oceram.2021.100058

An, X., Mu, Y., Liang, J., Li, J., Zhou, Y., and Sun, X. (2022). Stereolithography 3D printing of ceramic cores for hollow aeroengine turbine blades. *J. Mater Sci. Technol.* 127, 177–182. doi:10.1016/j.jmst.2022.01.042

ASTM C1161 (2023). *Standard test method for flexural strength of advanced ceramics at ambient temperature*. doi:10.1520/C1161-18R23

ASTM C1421 (2023). *Standard test methods for determination of fracture toughness of advanced ceramics at ambient temperature*. doi:10.1520/C1421-18

ASTM C1499-19 (2019). *Standard test method for monotonic equibiaxial flexural strength of advanced ceramics at ambient temperature*.

ASTM ISO/(2022). *Additive manufacturing - general principles - fundamental and vocabulary*.

Bae, C. J., and Halloran, J. W. (2011). Integrally cored ceramic mold fabricated by ceramic stereolithography. *Int. J. Appl. Ceram. Technol.* 8, 1255–1262. doi:10.1111/j.1744-7402.2010.02568.x

Bahraminasab, M. (2020). Challenges on optimization of 3D-printed bone scaffolds. *Biomed. Eng. Online* 19, 69. doi:10.1186/s12938-020-00810-2

Baino, F., Fiume, E., Barberi, J., Kargozar, S., Marchi, J., Massera, J., et al. (2019). Processing methods for making porous bioactive glass-based scaffolds—a state-of-the-art review. *Int. J. Appl. Ceram. Technol.* 16, 1762–1796. doi:10.1111/ijac.13195

Baino, F., Magnaterra, G., Fiume, E., Schiavi, A., Tofan, L., Schwentenwein, M., et al. (2022). Digital light processing stereolithography of hydroxyapatite scaffolds with bone-like architecture, permeability, and mechanical properties. *J. Am. Ceram. Soc.* 105, 1648–1657. doi:10.1111/jace.17843

Barry, J. J. A., Evseev, A. V., Markov, M. A., Upton, C. E., Scotchford, C. A., Popov, V. K., et al. (2008). *In vitro* study of hydroxyapatite-based photocurable polymer composites prepared by laser stereolithography and supercritical fluid extraction. *Acta Biomater.* 4, 1603–1610. doi:10.1016/j.actbio.2008.05.024

Bergmann, G., Bender, A., Dymke, J., Duda, G., and Damm, P. (2016). Standardized loads acting in hip implants. *PLoS One* 11, e0155612. doi:10.1371/journal.pone.0155612

Bindl, A., and Mormann, W. H. (2005). Marginal and internal fit of all-ceramic CAD/CAM crown-copings on chamfer preparations. *J. Oral Rehabil.* 32, 441–447. doi:10.1111/j.1365-2842.2005.01446.x

Boretti, A., and Banik, B. K. (2021). Advances in hydrogen production from natural gas reforming. *Adv. Energy Sustain. Res.* 2, 2100097. doi:10.1002/aesr.202100097

Borlaf, M., Szubra, N., Serra-Capdevila, A., Kubiak, W. W., and Graule, T. (2020). Fabrication of ZrO2 and ATZ materials via UV-LCM-DLP additive manufacturing technology. *J. Eur. Ceram. Soc.* 40, 1574–1581. doi:10.1016/j.jeurceramsoc.2019.11.037

Bortzmeyer, D. (1995). "Dry pressing of ceramic powders," in *Ceramic processing* (Dordrecht: Springer Netherlands), 102–146. doi:10.1007/978-94-011-0531-6_4

Bove, A., Calignano, F., Galati, M., and Iuliano, L. (2022). Photopolymerization of ceramic resins by stereolithography process: A review. *Appl. Sci. Switz.* 12, 3591. doi:10.3390/app12073591

Cao, X. Q., Vassen, R., and Stoever, D. (2004). Ceramic materials for thermal barrier coatings. *J. Eur. Ceram. Soc.* 24, 1–10. doi:10.1016/S0955-2219(03)00129-8

Cawley, J. D. (1999). Solid freeform fabrication of ceramics. *Curr. Opin. Solid State Mater Sci.* 4, 483–489. doi:10.1016/S1359-0286(99)00055-8

Chandra Babu Naidu, K., and Suresh Kumar, N. (2020). "Applications of advanced ceramics in science, technology, and medicine," in *Frontiers in ceramic science*. Editors K. Chandra Babu Naidu and N. Suresh (Kumar Bentham Books).

Chaudhary, R., Fabbri, P., Leoni, E., Mazzanti, F., Akbari, R., and Antonini, C. (2022). Additive manufacturing by digital light processing: A review. *Prog. Addit. Manuf.* 8, 331–351. doi:10.1007/s40964-022-00336-0

Chen, A., Su, J., Li, Y., Zhang, H., Shi, Y., Yan, C., et al. (2023). 3D/4D printed bio-piezoelectric smart scaffolds for next-generation bone tissue engineering. *Int. J. Extreme Manuf.* 5, 032007. doi:10.1088/2631-7990/acd88f

Chen, F., Wu, Y.-R., Wu, J.-M., Zhu, H., Chen, S., Hua, S.-B., et al. (2021a). Preparation and characterization of ZrO2-Al2O3 bioceramics by stereolithography technology for dental restorations. *Addit. Manuf.* 44, 102055. doi:10.1016/j.addma.2021.102055

Chen, H., Guo, L., Zhu, W., and Li, C. (2022a). Recent advances in multi-material 3D printing of functional ceramic devices. *Polym. (Basel)* 14, 4635. doi:10.3390/polym14214635

Chen, Q., Schmidt, F., Görke, O., Asif, A., Weinhold, J., Aghaei, E., et al. (2022c). Ceramic stereolithography of bioactive glasses: influence of resin composition on curing behavior and green body properties. *Biomedicines* 10, 395. doi:10.3390/biomedicines10020395

Chen, Y.-W., Moussi, J., Drury, J. L., and Wataha, J. C. (2016a). Zirconia in biomedical applications. *Expert Rev. Med. Devices* 13, 945–963. doi:10.1080/17434440.2016.1230017

Chen, Y., Wang, N., Ola, O., Xia, Y., and Zhu, Y. (2021b). Porous ceramics: light in weight but heavy in energy and environment technologies. *Mater. Sci. Eng. R Rep.* 143, 100589. doi:10.1016/j.mser.2020.100589

Chen, Z., Li, J., Liu, C., Liu, Y., Zhu, J., and Lao, C. (2019). Preparation of high solid loading and low viscosity ceramic slurries for photopolymerization-based 3D printing. *Ceram. Int.* 45, 11549–11557. doi:10.1016/j.ceramint.2019.03.024

Chen, Z., Song, X., Lei, L., Chen, X., Fei, C., Chiu, C. T., et al. (2016b). 3D printing of piezoelectric element for energy focusing and ultrasonic sensing. *Nano Energy* 27, 78–86. doi:10.1016/j.nanoen.2016.06.048

Chevalier, J., and Gremillard, L. (2009). Ceramics for medical applications: A picture for the next 20 years. *J. Eur. Ceram. Soc.* 29, 1245–1255. doi:10.1016/j.jeurceramsoc.2008.08.025

Chevalier, J., Gremillard, L., Virkar, A. V., and Clarke, D. R. (2009). The tetragonal-monoclinic transformation in zirconia: lessons learned and future trends. *J. Am. Ceram. Soc.* 92, 1901–1920. doi:10.1111/j.1551-2916.2009.03278.x

Chevalier, J., and Gremillard, L. (2008). "Zirconia ceramics," in *Bioceramics and their clinical applications* (China: Elsevier), 243–265. doi:10.1533/9781845694227.2.243

Chevarin, C., Wang, X., Bouyer, D., Tarabara, V., Chartier, T., and Ayral, A. (2023). CFD-guided patterning of tubular ceramic membrane surface by stereolithography: optimizing morphology at the mesoscale for improved hydrodynamic control of membrane fouling. *J. Memb. Sci.* 672, 121435. doi:10.1016/j.memsci.2023.121435

Coppola, B., Lacondemine, T., Tardivat, C., Montanaro, L., and Palmero, P. (2021). Designing alumina-zirconia composites by DLP-based stereolithography: microstructural tailoring and mechanical performances. *Ceram. Int.* 47, 13457–13468. doi:10.1016/j.ceramint.2021.01.204

Coppola, B., Montanaro, L., and Palmero, P. (2022a). DLP fabrication of zirconia scaffolds coated with HA/β-TCP layer: role of scaffold architecture on mechanical and biological properties. *J. Funct. Biomater.* 13, 148. doi:10.3390/jfb13030148

Coppola, B., Schmitt, J., Lacondemine, T., Tardivat, C., Montanaro, L., and Palmero, P. (2022b). Digital light processing stereolithography of zirconia ceramics: slurry elaboration and orientation-reliant mechanical properties. *J. Eur. Ceram. Soc.* 42, 2974–2982. doi:10.1016/j.jeurceramsoc.2022.01.024

Cramer, C. L., Ionescu, E., Graczyk-Zajac, M., Nelson, A. T., Katoh, Y., Haslam, J. J., et al. (2022). Additive manufacturing of ceramic materials for energy applications: road map and opportunities. *J. Eur. Ceram. Soc.* 42, 3049–3088. doi:10.1016/j.jeurceramsoc.2022.01.058

D'Andrea, L., Gastaldi, D., Baino, F., Verné, E., Saccomano, G., D'Amico, L., et al. (2023). Mechanical characterization of miniaturized 3D-printed hydroxyapatite parts obtained through vat photopolymerization: an experimental study. *J. Mech. Behav. Biomed. Mater* 141, 105760. doi:10.1016/j.jmbbm.2023.105760

De Hazan, Y., and Penner, D. (2017). SiC and SiOC ceramic articles produced by stereolithography of acrylate modified polycarbosilane systems. *J. Eur. Ceram. Soc.* 37, 5205–5212. doi:10.1016/j.jeurceramsoc.2017.03.021

Dehurtevent, M., Robberecht, L., Hornez, J. C., Thuault, A., Deveaux, E., and Béhin, P. (2017). Stereolithography: A new method for processing dental ceramics by additive computer-aided manufacturing. *Dent. Mater.* 33, 477–485. doi:10.1016/j.dental.2017.01.018

Denis, C., Robberecht, L., Delattre, J., Deveaux, E., Hornez, J.-C., and Dehurtevent, M. (2023). Effect of dimensional variations on the manufacturing process and the 3D shrinkage ratio of stereolithographic dental alumina ceramics. *Dent. Mater J.* 42, 79–85. doi:10.4012/dmj.2022-102

Dimopoulos Eggenschwiler, P., Tsinoglou, D. N., Seyfert, J., Bach, C., Vogt, U., and Gorbar, M. (2009). Ceramic foam substrates for automotive catalyst applications: fluid mechanic analysis. *Exp. Fluids* 47, 209–222. doi:10.1007/s00348-009-0653-2

Ding, G., He, R., Zhang, K., Xia, M., Feng, C., and Fang, D. (2020a). Dispersion and stability of SiC ceramic slurry for stereolithography. *Ceram. Int.* 46, 4720–4729. doi:10.1016/j.ceramint.2019.10.203

Ding, G., He, R., Zhang, K., Zhou, N., and Xu, H. (2020b). Stereolithography 3D printing of SiC ceramic with potential for lightweight optical mirror. *Ceram. Int.* 46, 18785–18790. doi:10.1016/j.ceramint.2020.04.196

Ding, Z., Zreiqat, H., and Mirkhalaf, M. (2022). Rationally-designed self-shaped ceramics through heterogeneous green body compositions. *Mater Horiz.* 9, 2762–2772. doi:10.1039/D2MH00785A

Dong, Z., and Zhao, X. (2021). Application of TPMS structure in bone regeneration. *Eng. Regen.* 2, 154–162. doi:10.1016/j.engreg.2021.09.004

Dou, R., Tang, W., Hu, K., and Wang, L. (2022). Ceramic paste for space stereolithography 3D printing technology in microgravity environment. *J. Eur. Ceram. Soc.* 42, 3968–3975. doi:10.1016/j.jeurceramsoc.2022.03.030

Edirisinghe, M. J., and Evans, J. R. G. (1986). Review: fabrication of engineering ceramics by injection moulding. I. Materials selection. *Int. J. High Technol. Ceram.* 2, 1–31. doi:10.1016/0267-3762(86)90002-0

Fan, J., Xu, X., Niu, S., Zhou, Y., Li, X., Guo, Y., et al. (2022). Anisotropy management on microstructure and mechanical property in 3D printing of silica-based ceramic cores. *J. Eur. Ceram. Soc.* 42, 4388–4395. doi:10.1016/j.jeurceramsoc.2022.03.059

Feng, J., Fu, J., Lin, Z., Shang, C., and Li, B. (2018). A review of the design methods of complex topology structures for 3D printing. *Vis. Comput. Ind. Biomed. Art.* 1, 5. doi:10.1186/s42492-018-0004-3

Fiume, E., Ciavattini, S., Verné, E., and Baino, F. (2021). Foam replica method in the manufacturing of bioactive glass scaffolds: out-of-Date technology or still underexploited potential? *Materials* 14, 2795. doi:10.3390/ma14112795

Fournier, S., Chevalier, J., Baeza, G. P., Chaput, C., Louradour, E., Sainsot, P., et al. (2023). Ceria-stabilized zirconia-based composites printed by stereolithography: impact of the processing method on the ductile behaviour and its transformation features. *J. Eur. Ceram. Soc.* 43, 2894–2906. doi:10.1016/j.jeurceramsoc.2022.11.006

Gan, Z., Turner, M. D., and Gu, M. (2016). Biomimetic gyroid nanostructures exceeding their natural origins. *Sci. Adv.* 2, e1600084. doi:10.1126/sciadv.1600084

Gentry, S. P., and Halloran, J. W. (2013). Depth and width of cured lines in photopolymerizable ceramic suspensions. *J. Eur. Ceram. Soc.* 33, 1981–1988. doi:10.1016/j.jeurceramsoc.2013.02.033

Gerhardt, L.-C., and Boccaccini, A. R. (2010). Bioactive glass and glass-ceramic scaffolds for bone tissue engineering. *Materials* 3, 3867–3910. doi:10.3390/ma3073867

Gervaso, F., Scalera, F., Kunjalukkal Padmanabhan, S., Sannino, A., and Licciulli, A. (2012). High-performance hydroxyapatite scaffolds for bone tissue engineering applications. *Int. J. Appl. Ceram. Technol.* 9, 507–516. doi:10.1111/j.1744-7402.2011.02662.x

Gmeiner, R., Mitteramskogler, G., Stampfl, J., and Boccaccini, A. R. (2015). Stereolithographic ceramic manufacturing of high strength bioactive glass. *Int. J. Appl. Ceram. Technol.* 12, 38–45. doi:10.1111/ijac.12325

Griffith, M. L., and Halloran, J. W. (1994). *Ultraviolet curing of highly loaded ceramic suspensions for stereolithography of ceramics*, 396–403.

Gu, Y., Duan, W., Wang, T., Liu, X., Li, S., Liu, B., et al. (2023). Additive manufacturing of Al2O3 ceramic core with applicable microstructure and mechanical properties via digital light processing of high solid loading slurry. *Ceram. Int.* 49, 25216–25224. doi:10.1016/j.ceramint.2023.05.054

Han, Z., Liu, S., Qiu, K., Liu, J., Zou, R., Wang, Y., et al. (2023). The enhanced ZrO2 produced by DLP via a reliable plasticizer and its dental application. *J. Mech. Behav. Biomed. Mater* 141, 105751. doi:10.1016/j.jmbbm.2023.105751

Hannink, R. H. J., Kelly, P. M., and Muddle, B. C. (2004). Transformation toughening in zirconia-containing ceramics. *J. Am. Ceram. Soc.* 83, 461–487. doi:10.1111/j.1151-2916.2000.tb01221.x

Hench, L. L., and Kokubo, T. (1998). "Properties of bioactive glasses and glass-ceramics," in *Handbook of biomaterial properties* (Boston, MA: Springer US), 355–363. doi:10.1007/978-1-4615-5801-9_22

Hinczewski, C., Corbel, S., and Chartier, T. (1998). Ceramic suspensions suitable for stereolithography. *J. Eur. Ceram. Soc.* 18, 583–590. doi:10.1016/S0955-2219(97)00186-6

Hu, K., Zhao, P., Li, J., and Lu, Z. (2022). High-resolution multiceramic additive manufacturing based on digital light processing. *Addit. Manuf.* 54, 102732. doi:10.1016/j.addma.2022.102732

Hull, C. (1988). StereoLithography: plastic prototypes from CAD data without tooling. *Mod. Cast.* 78, 38.

Hull, C. W. (1986). *Apparatus for production of three-dimensional objects by stereolithography*.

Humphreys, C. J. (1991). "Ceramic superconductors," in *Concise encyclopedia of advanced ceramic materials*. Editor R. J. Brooke (Turkey: Pergamon), 67–73.

Inserra, B., Coppola, B., Montanaro, L., Tulliani, J.-M., and Palmero, P. (2023). Preparation and characterization of Ce-ZrO2/Al2O3 composites by DLP-based stereolithography. *J. Eur. Ceram. Soc.* 43, 2907–2916. doi:10.1016/j.jeurceramsoc.2022.08.037

Isachenkov, M., Chugunov, S., Akhatov, I., and Shishkovsky, I. (2021). Regolith-based additive manufacturing for sustainable development of lunar infrastructure – an overview. *Acta Astronaut.* 180, 650–678. doi:10.1016/j.actaastro.2021.01.005

Ishikawa, K., Matsuya, S., Miyamoto, Y., and Kawate, K. (2003). "Bioceramics," in *Comprehensive structural integrity* (Netherlands: Elsevier), 169–214. doi:10.1016/B0-08-043749-4/09146-1

Iulianelli, A., Ribeirinha, P., Mendes, A., and Basile, A. (2014). Methanol steam reforming for hydrogen generation via conventional and membrane reactors: A review. *Renew. Sustain. Energy Rev.* 29, 355–368. doi:10.1016/j.rser.2013.08.032

Jabbari, M., Bulatova, R., Tok, A. I. Y., Bahl, C. R. H., Mitsoulis, E., and Hattel, J. H. (2016). Ceramic tape casting: A review of current methods and trends with emphasis on rheological behaviour and flow analysis. *Mater. Sci. Eng. B* 212, 39–61. doi:10.1016/j.mseb.2016.07.011

Jaeger, J. (2021). *Explaining the exponential growth of renewable energy*.

Jia, K., Zheng, L., Liu, W., Zhang, J., Yu, F., Meng, X., et al. (2022). A new and simple way to prepare monolithic solid oxide fuel cell stack by stereolithography 3D printing technology using 8 mol% yttria stabilized zirconia photocurable slurry. *J. Eur. Ceram. Soc.* 42, 4275–4285. doi:10.1016/j.jeurceramsoc.2022.03.060

Jiang, D., Zeng, Y., Singh, M., and Heinrich, J. (2010). in *Ceramic materials and components for energy and environmental applications ceramic transactions series*. Editors D. Jiang, Y. Zeng, M. Singh, and J. Heirich (Hoboken: John Wiley and Sons).

Jiang, H., Zou, Y. K., Chen, Q., Li, K. K., Zhang, R., Wang, Y., et al. (2005). "Proc. SPIE 5644, Optoelectonic device and integration," in *Transparent electro-optic ceramics and devices*, 380. doi:10.1117/12.582105

Jiang, Z., Cheng, L., Zeng, Y., Zhang, Z., Zhao, Y., Dong, P., et al. (2022). 3D printing of porous scaffolds BaTiO3 piezoelectric ceramics and regulation of their mechanical and electrical properties. *Ceram. Int.* 48, 6477–6487. doi:10.1016/j.ceramint.2021.11.192

Jung, J.-M., Kim, G.-N., Koh, Y.-H., and Kim, H.-E. (2023). Manufacturing and characterization of dental crowns made of 5-mol% yttria stabilized zirconia by digital light processing. *Materials* 16, 1447. doi:10.3390/ma16041447

Kang, J.-H., Sakthiabirami, K., Jang, K.-J., Jang, J.-G., Oh, G.-J., Park, C., et al. (2022). Mechanical and biological evaluation of lattice structured hydroxyapatite scaffolds produced via stereolithography additive manufacturing. *Mater Des.* 214, 110372. doi:10.1016/j.matdes.2021.110372

Kanyo, J. E., Schafföner, S., Uwanyuze, R. S., and Leary, K. S. (2020). An overview of ceramic molds for investment casting of nickel superalloys. *J. Eur. Ceram. Soc.* 40, 4955–4973. doi:10.1016/j.jeurceramsoc.2020.07.013

Karkun, M. S., and Dharmalinga, S. (2022). 3D printing technology in aerospace industry – a review. *Int. J. Aviat. Aeronautics, Aerosp.* doi:10.15394/ijaaa.2022.1708

Kaur, G., Pandey, O. P., Singh, K., Homa, D., Scott, B., and Pickrell, G. (2014). A review of bioactive glasses: their structure, properties, fabrication and apatite formation. *J. Biomed. Mater Res. A* 102, 254–274. doi:10.1002/jbm.a.34690

Khalile, N., Meunier, C., Petit, C., Valdivieso, F., Coppola, B., and Palmero, P. (2023). Microwave sintering of dense and lattice 3Y-TZP samples shaped by digital light processing. *Ceram. Int.* 49, 7350–7358. doi:10.1016/j.ceramint.2022.10.194

Khanlar, L. N., Rios, A. S., Tahmaseb, A., and Zandinejad, A. (2021). Additive manufacturing of zirconia ceramic and its application in clinical dentistry: A review. *Dent. J. (Basel)* 9, 104. doi:10.3390/DJ9090104

Kim, J.-W., Yang, B.-E., Hong, S.-J., Choi, H.-G., Byeon, S.-J., Lim, H.-K., et al. (2020). Bone regeneration capability of 3D printed ceramic scaffolds. *Int. J. Mol. Sci.* 21, 4837. doi:10.3390/ijms21144837

Kim, J., Choi, Y., Gal, C. W., Park, H., Yoon, S., and Yun, H. (2022). Effect of dispersants on structural integrity of 3D printed ceramics. *Int. J. Appl. Ceram. Technol.* 19, 968–978. doi:10.1111/ijac.13965

Kim, K., Yeatts, A., Dean, D., and Fisher, J. P. (2010). Stereolithographic bone scaffold design parameters: osteogenic differentiation and signal expression. *Tissue Eng. Part B Rev.* 16, 523–539. doi:10.1089/ten.teb.2010.0171

Klauda, M., Kasser, T., Mayer, B., Neumann, C., Schnell, F., Aminov, B., et al. (2000). Superconductors and cryogenics for future communication systems. *IEEE Trans. Microw. Theory Tech.* 48, 1227–1239. doi:10.1109/22.853466

Kontonasaki, E., Giasimakopoulos, P., and Rigos, A. E. (2020). Strength and aging resistance of monolithic zirconia: an update to current knowledge. *Jpn. Dent. Sci. Rev.* 56, 1–23. doi:10.1016/j.jdsr.2019.09.002

Kovacev, N., Li, S., Zeraati-Rezaei, S., Hemida, H., Tsolakis, A., and Essa, K. (2021). Effects of the internal structures of monolith ceramic substrates on thermal and hydraulic properties: additive manufacturing, numerical modelling and experimental testing. *Int. J. Adv. Manuf. Technol.* 112, 1115–1132. doi:10.1007/s00170-020-06493-2

Kumar, L. J., and Krishnadas Nair, C. G. (2017). "Current trends of additive manufacturing in the aerospace industry," in *Advances in 3D printing and additive manufacturing technologies* (Singapore: Springer Singapore), 39–54. doi:10.1007/978-981-10-0812-2_4

Labhsetwar, N., Doggali, P., Rayalu, S., Yadav, R., Mistuhashi, T., and Haneda, H. (2012). Ceramics in environmental catalysis: applications and possibilities. *Cuihua Xuebao/Chinese J. Catal.* 33, 1611–1621. doi:10.1016/s1872-2067(11)60440-3

Lakhdar, Y., Tuck, C., Binner, J., Terry, A., and Goodridge, R. (2021). Additive manufacturing of advanced ceramic materials. *Prog. Mater Sci.* 116, 100736. doi:10.1016/j.pmatsci.2020.100736

Lamicq, P. (1999). Main features of thermostructural composites for space, aeronautic and industrial applications. *Adv. Compos. Mater.* 8, 47–53. doi:10.1163/156855199X00065

Lee, J.-B., Maeng, W.-Y., Koh, Y.-H., and Kim, H.-E. (2018). Porous calcium phosphate ceramic scaffolds with tailored pore orientations and mechanical properties using lithography-based ceramic 3D printing technique. *Materials* 11, 1711. doi:10.3390/ma11091711

Lee, K. N. (2000). Current status of environmental barrier coatings for Si-Based ceramics. *Surf. Coat. Technol.* 133, 1–7. doi:10.1016/S0257-8972(00)00889-6

LeGeros, R. Z. (2002). Properties of osteoconductive biomaterials: calcium phosphates. *Clin. Orthop. Relat. Res.* 395, 81–98. doi:10.1097/00003086-200202000-00009

Lei, H., Song, C., Liu, Z., Deng, Z., Yu, J., Yuan, F., et al. (2022). Rational design and additive manufacturing of alumina-based lattice structures for bone implant. *Mater Des.* 221, 111003. doi:10.1016/j.matdes.2022.111003

Li, H., Liu, Y., Liu, Y., Zeng, Q., Hu, K., Lu, Z., et al. (2020a). Effect of debinding temperature under an argon atmosphere on the microstructure and properties of 3D-printed alumina ceramics. *Mater Charact.* 168, 110548. doi:10.1016/j.matchar.2020.110548

Li, H., Liu, Y., Liu, Y., Zeng, Q., Wang, J., Hu, K., et al. (2020b). Evolution of the microstructure and mechanical properties of stereolithography formed alumina cores sintered in vacuum. *J. Eur. Ceram. Soc.* 40, 4825–4836. doi:10.1016/j.jeurceramsoc.2019.11.047

Li, H., Song, L., Sun, J., Ma, J., and Shen, Z. (2019). Dental ceramic prostheses by stereolithography-based additive manufacturing: potentials and challenges. *Adv. Appl. Ceram.* 118, 30–36. doi:10.1080/17436753.2018.1447834

Li, H., Song, L., Sun, J., Ma, J., and Shen, Z. (2020c). Stereolithography-fabricated zirconia dental prostheses: concerns based on clinical requirements. *Adv. Appl. Ceram.* 119, 236–243. doi:10.1080/17436753.2019.1709687

Li, Q., An, X., Liang, J., Liu, Y., Hu, K., Lu, Z., et al. (2022a). Balancing flexural strength and porosity in DLP-3D printing Al2O3 cores for hollow turbine blades. *J. Mater Sci. Technol.* 104, 19–32. doi:10.1016/j.jmst.2021.05.077

Li, Q., Hou, W., Liang, J., Zhang, C., Li, J., Zhou, Y., et al. (2022b). Controlling the anisotropy behaviour of 3D printed ceramic cores: from intralayer particle distribution to interlayer pore evolution. *Addit. Manuf.* 58, 103055. doi:10.1016/j.addma.2022.103055

Li, Q., Meng, X., Zhang, X., Liang, J., Zhang, C., Li, J., et al. (2022c). Enhanced 3D printed Al2O3 core via *in-situ* mullite. *Addit. Manuf.* 55, 102826. doi:10.1016/j.addma.2022.102826

Li, S., Duan, W., Zhao, T., Han, W., Wang, L., Dou, R., et al. (2018). The fabrication of SiBCN ceramic components from preceramic polymers by digital light processing (DLP) 3D printing technology. *J. Eur. Ceram. Soc.* 38, 4597–4603. doi:10.1016/j.jeurceramsoc.2018.06.046

Li, T., Liu, Q., Qi, H., and Zhai, W. (2022d). Prestrain programmable 4D printing of nanoceramic composites with bioinspired microstructure. *Small* 18, e2204032. doi:10.1002/smll.202204032

Li, W., Liu, M., Liu, W., Zhou, H., Li, M., Chen, Y., et al. (2022e). High-performance integrated manufacturing of a 3Y-TZP ceramic crown through viscoelastic paste-based vat photopolymerization with a conformal contactless support. *Addit. Manuf.* 59, 103143. doi:10.1016/j.addma.2022.103143

Lian, Q., Sui, W., Wu, X., Yang, F., and Yang, S. (2018). Additive manufacturing of ZrO2 ceramic dental bridges by stereolithography. *Rapid Prototyp. J.* 24, 114–119. doi:10.1108/RPJ-09-2016-0144

CeraFab Multi 2M30-For innovators, by innovators (2023). Available at: https://lithoz.com/en/3d-printer/cerafab-multi/ (Last access September 26, 2023).

Liu, G., Zhao, Y., Wu, G., and Lu, J. (2018). Origami and 4D printing of elastomer-derived ceramic structures. *Sci. Adv.* 4, eaat0641. doi:10.1126/sciadv.aat0641

Liu, K., Zhou, C., Hu, J., Zhang, S., Zhang, Q., Sun, C., et al. (2021a). Fabrication of barium titanate ceramics via digital light processing 3D printing by using high refractive index monomer. *J. Eur. Ceram. Soc.* 41, 5909–5917. doi:10.1016/j.jeurceramsoc.2021.04.044

Liu, R., Ma, L., Liu, H., Xu, B., Feng, C., and He, R. (2021b). Effects of pore size on the mechanical and biological properties of stereolithographic 3D printed HAp bioceramic scaffold. *Ceram. Int.* 47, 28924–28931. doi:10.1016/j.ceramint.2021.07.053

Liu, S., Chen, J., Chen, T., and Zeng, Y. (2021c). Fabrication of trabecular-like beta-tricalcium phosphate biomimetic scaffolds for bone tissue engineering. *Ceram. Int.* 47, 13187–13198. doi:10.1016/j.ceramint.2021.01.184

Liu, X., Zou, B., Xing, H., and Huang, C. (2020). The preparation of ZrO2-Al2O3 composite ceramic by SLA-3D printing and sintering processing. *Ceram. Int.* 46, 937–944. doi:10.1016/j.ceramint.2019.09.054

Lu, S., Zhang, M., Guo, S., Hur, B., and Yue, X. (2022). Numerical investigation of impact behavior of strut-based cellular structures designed by spatial Voronoi tessellation. *Met. (Basel)* 12, 1189. doi:10.3390/met12071189

Lu, Z. L., Cao, J. W., Jing, H., Liu, T., Lu, F., Wang, D. X., et al. (2013). Review of main manufacturing processes of complex hollow turbine blades: this paper critically reviews conventional and advanced technologies used for manufacturing hollow turbine blades. *Virtual Phys. Prototyp.* 8, 87–95. doi:10.1080/17452759.2013.790600

Lu, Z. L., Fan, Y. X., Miao, K., Jing, H., and Li, D. C. (2014). Effects of adding aluminum oxide or zirconium oxide fibers on ceramic molds for casting hollow turbine blades. *Int. J. Adv. Manuf. Technol.* 72, 873–880. doi:10.1007/s00170-014-5723-9

Lucci, F., Della Torre, A., Montenegro, G., and Dimopoulos Eggenschwiler, P. (2015). On the catalytic performance of open cell structures versus honeycombs. *Chem. Eng. J.* 264, 514–521. doi:10.1016/j.cej.2014.11.080

Manière, C., Kerbart, G., Harnois, C., and Marinel, S. (2020). Modeling sintering anisotropy in ceramic stereolithography of silica. *Acta Mater* 182, 163–171. doi:10.1016/j.actamat.2019.10.032

Martinez, D. W., Espino, M. T., Cascolan, H. M., Crisostomo, J. L., and Dizon, J. R. C. (2022a). A comprehensive review on the application of 3D printing in the aerospace industry. *Key Eng. Mater* 913, 27–34. doi:10.4028/p-94a9zb

Martinez, J. S., Peterson, S., Hoel, C. A., Erno, D. J., Murray, T., Boyd, L., et al. (2022b). High resolution DLP stereolithography to fabricate biocompatible hydroxyapatite structures that support osteogenesis. *PLoS One* 17, e0272283. doi:10.1371/journal.pone.0272283

Masciandaro, S., Torrell, M., Leone, P., and Tarancón, A. (2019). Three-dimensional printed yttria-stabilized zirconia self-supported electrolytes for solid oxide fuel cell applications. *J. Eur. Ceram. Soc.* 39, 9–16. doi:10.1016/j.jeurceramsoc.2017.11.033

Maskery, I., Sturm, L., Aremu, A. O., Panesar, A., Williams, C. B., Tuck, C. J., et al. (2018). Insights into the mechanical properties of several triply periodic minimal surface lattice structures made by polymer additive manufacturing. *Polym. Guildf.* 152, 62–71. doi:10.1016/j.polymer.2017.11.049

Meng, J., Lian, Q., Xi, S., Yi, Y., Lu, Y., and Wu, G. (2022). Crown fit and dimensional accuracy of zirconia fixed crowns based on the digital light processing technology. *Ceram. Int.* 48, 17852–17863. doi:10.1016/j.ceramint.2022.03.057

Mohammadi, M., Coppola, B., Montanaro, L., and Palmero, P. (2023). Digital light processing of high-strength hydroxyapatite ceramics: role of particle size and printing parameters on microstructural defects and mechanical properties. *J. Eur. Ceram. Soc.* 43, 2761–2772. doi:10.1016/j.jeurceramsoc.2022.11.047

Montanaro, L., Palmero, P., Chevalier, J., Reveron, H., and Fuerderer, T. (2018). *Process for producing zirconia-based multi-phasic ceramic composites*.

Muhammad Syazwan, M. N., Ahmad-Fauzi, M. N., Balestri, W., Reinwald, Y., and Yanny Marliana, B. I. (2021). Effectiveness of various sintering aids on the densification and *in vitro* properties of carbonated hydroxyapatite porous scaffolds produced by foam

replication technique. *Mater Today Commun.* 27, 102395. doi:10.1016/j.mtcomm.2021.102395

Najmon, J. C., Raeisi, S., and Tovar, A. (2019). "Review of additive manufacturing technologies and applications in the aerospace industry," in *Additive manufacturing for the aerospace industry* (Netherlands: Elsevier), 7–31. doi:10.1016/B978-0-12-814062-8.00002-9

Naveen Kumar, K., Gopalsamy, M., Antony, D., Krishnaraj, R., and Viswanadh, C. B. V. (2017). Design and optimization of aerospike nozzle using CFD. *IOP Conf. Ser. Mater Sci. Eng.* 247, 012008. doi:10.1088/1757-899X/247/1/012008

Nevarez-Rascon, A., Aguilar-Elguezabal, A., Orrantia, E., and Bocanegra-Bernal, M. H. (2009). On the wide range of mechanical properties of ZTA and ATZ based dental ceramic composites by varying the Al2O3 and ZrO2 content. *Int. J. Refract Met. Hard Mater* 27, 962–970. doi:10.1016/j.ijrmhm.2009.06.001

Ni, M., Leung, M. K. H., Leung, D. Y. C., and Sumathy, K. (2007). A review and recent developments in photocatalytic water-splitting using TiO2 for hydrogen production. *Renew. Sustain. Energy Rev.* 11, 401–425. doi:10.1016/j.rser.2005.01.009

Niu, S., Luo, Y., Li, X., Chen, Y., Cheng, Y., Dai, S., et al. (2022). 3D printing of silica-based ceramic cores reinforced by alumina with controlled anisotropy. *J. Alloys Compd.* 922, 166325. doi:10.1016/j.jallcom.2022.166325

Oonishi, H., Hench, L. L., Wilson, J., Sugihara, F., Tsuji, E., Matsuura, M., et al. (2000). Quantitative comparison of bone growth behavior in granules of Bioglass, A-W glass-ceramic, and hydroxyapatite. *J. Biomed. Mater Res.* 51, 37–46. doi:10.1002/(SICI)1097-4636

Palmero, P., Fornabaio, M., Montanaro, L., Reveron, H., Esnouf, C., and Chevalier, J. (2015). Towards long lasting zirconia-based composites for dental implants. Part I: innovative synthesis, microstructural characterization and *in vitro* stability. *Biomaterials* 50, 38–46. doi:10.1016/j.biomaterials.2015.01.018

Pan, C., Han, Y., and Lu, J. (2020). Design and optimization of lattice structures: A review. *Appl. Sci.* 10, 6374. doi:10.3390/app10186374

Pan, Y., and Chen, Y. (2016). Meniscus process optimization for smooth surface fabrication in Stereolithography. *Addit. Manuf.* 12, 321–333. doi:10.1016/j.addma.2016.05.004

Papetti, V., Dimopoulos Eggenschwiler, P., Della Torre, A., Lucci, F., Ortona, A., and Montenegro, G. (2018). Additive Manufactured open cell polyhedral structures as substrates for automotive catalysts. *Int. J. Heat. Mass Transf.* 126, 1035–1047. doi:10.1016/j.ijheatmasstransfer.2018.06.061

Park, G.-S., Kim, S.-K., Heo, S.-J., Koak, J.-Y., and Seo, D.-G. (2019). Effects of printing parameters on the fit of implant-supported 3D printing resin prosthetics. *Materials* 12, 2533. doi:10.3390/ma12162533

Pelanconi, M., and Ortona, A. (2019). Nature-inspired, ultra-lightweight structures with gyroid cores produced by additive manufacturing and reinforced by unidirectional carbon fiber ribs. *Materials* 12, 4134. doi:10.3390/ma12244134

Pesce, A., Hornés, A., Núñez, M., Morata, A., Torrell, M., and Tarancón, A. (2020). 3D printing the next generation of enhanced solid oxide fuel and electrolysis cells. *J. Mater Chem. A Mater* 8, 16926–16932. doi:10.1039/d0ta02803g

Piconi, C., and Sprio, S. (2021). Oxide bioceramic composites in orthopedics and dentistry. *J. Compos. Sci.* 5, 206. doi:10.3390/jcs5080206

Pollinger, J. P., Khalfalla, Y. E., and Benyounis, K. Y. (2016). "Gel casting," in *Reference module in materials science and materials engineering* (Netherlands: Elsevier). doi:10.1016/B978-0-12-803581-8.03556-6

Prakoso, A. T., Basri, H., Adanta, D., Yani, I., Ammarullah, M. I., Akbar, I., et al. (2023). The effect of tortuosity on permeability of porous scaffold. *Biomedicines* 11, 427. doi:10.3390/biomedicines11020427

Qin, Y., and Pan, W. (2009). Effect of silica sol on the properties of alumina-based ceramic core composites. *Mater. Sci. Eng. A* 508, 71–75. doi:10.1016/j.msea.2008.12.016

Rahmati, M., and Mozafari, M. (2019). Biocompatibility of alumina-based biomaterials–A review. *J. Cell. Physiol.* 234, 3321–3335. doi:10.1002/jcp.27292

Rakshit, R., and Das, A. K. (2019). A review on cutting of industrial ceramic materials. *Precis. Eng.* 59, 90–109. doi:10.1016/j.precisioneng.2019.05.009

Reveron, H., Fornabaio, M., Palmero, P., Fürderer, T., Adolfsson, E., Lughi, V., et al. (2017). Towards long lasting zirconia-based composites for dental implants: transformation induced plasticity and its consequence on ceramic reliability. *Acta Biomater.* 48, 423–432. doi:10.1016/j.actbio.2016.11.040

Revilla-León, M., Mostafavi, D., Methani, M. M., and Zandinejad, A. (2022). Manufacturing accuracy and volumetric changes of stereolithography additively manufactured zirconia with different porosities. *J. Prosthet. Dent.* 128, 211–215. doi:10.1016/j.prosdent.2020.06.021

Roddy, E., DeBaun, M. R., Daoud-Gray, A., Yang, Y. P., and Gardner, M. J. (2018). Treatment of critical-sized bone defects: clinical and tissue engineering perspectives. *Eur. J. Orthop. Surg. Traumatology* 28, 351–362. doi:10.1007/s00590-017-2063-0

Rokhvarger, A. E., and Chigirinsky, L. A. (2004). Engineering of superconductive ceramics. *J. Electron Packag* 126, 26–33. doi:10.1115/1.1646423

Rüegsegger, P., Durand, E. P., and Dambacher, M. A. (1991). Differential effects of aging and disease on trabecular and compact bone density of the radius. *Bone* 12, 99–105. doi:10.1016/8756-3282(91)90007-6

Ruiz-Morales, J. C., Tarancón, A., Canales-Vázquez, J., Méndez-Ramos, J., Hernández-Afonso, L., Acosta-Mora, P., et al. (2017). Three dimensional printing of components and functional devices for energy and environmental applications. *Energy Environ. Sci.* 10, 846–859. doi:10.1039/c6ee03526d

Safonov, A., Maltsev, E., Chugunov, S., Tikhonov, A., Konev, S., Evlashin, S., et al. (2020). Design and fabrication of complex-shaped ceramic bone implants via 3D printing based on laser stereolithography. *Appl. Sci.* 10, 7138. doi:10.3390/app10207138

Salame, P. H., and Kolte, J. T. (2020). "Role of lanthanide substitution on suitable sites in enhancing the properties of various electroceramics," in *Spectroscopy of lanthanide doped oxide materials*. Editors S. J. Dhoble, V. B. Pawade, H. C. Swart, and V. Chopra (Netherlands: Elsevier), 365–392. doi:10.1016/B978-0-08-102935-0.00011-3

Santoliquido, O., Camerota, F., Pelanconi, M., Ferri, D., Elsener, M., Eggenschwiler, P. D., et al. (2021). Structured alumina substrates for environmental catalysis produced by stereolithography. *Appl. Sci. Switz.* 11, 8239. doi:10.3390/app11178239

Schoenung, J. M. (2001). "Structural ceramics," in *Encyclopedia of materials: Science and technology*. K. H. J. Buschow, R. W. Cahn, M. C. Flemings, B. Ilschner, E. J. Kramer, and S. Mahajan Editors (Netherlands: Elsevier), 8921–8926.

Schwarzer, E., Holtzhausen, S., Scheithauer, U., Ortmann, C., Oberbach, T., Moritz, T., et al. (2019). Process development for additive manufacturing of functionally graded alumina toughened zirconia components intended for medical implant application. *J. Eur. Ceram. Soc.* 39, 522–530. doi:10.1016/j.jeurceramsoc.2018.09.003

Schwarzer-Fischer, E., Abel, J., Sieder-Katzmann, J., Propst, M., Bach, C., Scheithauer, U., et al. (2022). Study on CerAMfacturing of novel alumina aerospike nozzles by lithography-based ceramic vat photopolymerization (CerAM VPP). *Materials* 15, 3279. doi:10.3390/ma15093279

Seharing, A., Azman, A. H., and Abdullah, S. (2020). A review on integration of lightweight gradient lattice structures in additive manufacturing parts. *Adv. Mech. Eng.* 12, 168781402091695. doi:10.1177/1687814020916951

Shabani, S., Naghizadeh, R., Golestanifard, F., Fallah Vostakola, M., and Ghasemi, E. (2019). Effect of TiO_2 addition on microstructure and mechanical properties of alumina-based cores prepared by sol-gel method. *Int. J. Appl. Ceram. Technol.* 16, 2409–2418. doi:10.1111/ijac.13268

Shahmiri, R., Standard, O. C., Hart, J. N., and Sorrell, C. C. (2018). Optical properties of zirconia ceramics for esthetic dental restorations: A systematic review. *J. Prosthet. Dent.* 119, 36–46. doi:10.1016/j.prosdent.2017.07.009

Shapiro, A. A., Borgonia, J. P., Chen, Q. N., Dillon, R. P., McEnerney, B., Polit-Casillas, R., et al. (2016). Additive manufacturing for aerospace flight applications. *J. Spacecr. Rockets* 53, 952–959. doi:10.2514/1.A33544

Shaukat, U., Rossegger, E., and Schlögl, S. (2022a). A review of multi-material 3D printing of functional materials via vat photopolymerization. *Polym. (Basel)* 14, 2449. doi:10.3390/polym14122449

Shekhawat, D., Singh, A., Banerjee, M. K., Singh, T., and Patnaik, A. (2021). Bioceramic composites for orthopaedic applications: A comprehensive review of mechanical, biological, and microstructural properties. *Ceram. Int.* 47, 3013–3030. doi:10.1016/j.ceramint.2020.09.214

Shiraishi, T., and Watanabe, I. (2016). Thickness dependence of light transmittance, translucency and opalescence of a ceria-stabilized zirconia/alumina nanocomposite for dental applications. *Dent. Mater.* 32, 660–667. doi:10.1016/j.dental.2016.02.004

Shrirao, P. N., and Pawar, A. N. (2011). Evaluation of performance and emission characteristics of turbocharged diesel engine with mullite as thermal barrier coating. Available at: https://www.researchgate.net/publication/266329859.

Singh, K., Kaur, M., and Kumar, A. (2021). "Progress in advanced ceramics: energy and environmental perspective," in *Advanced ceramics for energy and environmental applications*. Editor A. Kumar (Boca Raton: CRC Press).

Soboyejo, W. O., Obayemi, J. D., Annan, E., Ampaw, E. K., Daniels, L., and Rahbar, N. (2015). Review of high temperature ceramics for aerospace applications. *Adv. Mat. Res.* 1132, 385–407. doi:10.4028/www.scientific.net/amr.1132.385

Spirrett, F., Ito, T., and Kirihara, S. (2022). High-speed alumina stereolithography. *Appl. Sci.* 12, 9760. doi:10.3390/app12199760

Steinfeld, A. (2005). Solar thermochemical production of hydrogen - a review. *Sol. Energy* 78, 603–615. doi:10.1016/j.solener.2003.12.012

Steyer, T. E. (2013). Shaping the future of ceramics for aerospace applications. *Int. J. Appl. Ceram. Technol.* 10, 389–394. doi:10.1111/ijac.12069

Studart, A. R., Filser, F., Kocher, P., and Gauckler, L. J. (2007). *In vitro* lifetime of dental ceramics under cyclic loading in water. *Biomaterials* 28, 2695–2705. doi:10.1016/j.biomaterials.2006.12.033

Su, C.-Y., Wang, J.-C., Chen, D.-S., Chuang, C.-C., and Lin, C.-K. (2020). Additive manufacturing of dental prosthesis using pristine and recycled zirconia solvent-based slurry stereolithography. *Ceram. Int.* 46, 28701–28709. doi:10.1016/j.ceramint.2020.08.030

Su, J., Hua, S., Chen, A., Chen, P., Yang, L., Yuan, X., et al. (2022). Three-dimensional printing of gyroid-structured composite bioceramic scaffolds with tuneable degradability. *Biomater. Adv.* 133, 112595. doi:10.1016/j.msec.2021.112595

Tang, J., Guo, X., Chang, H., Hu, K., Shen, Z., Wang, W., et al. (2021). The preparation of SiC ceramic photosensitive slurry for rapid stereolithography. *J. Eur. Ceram. Soc.* 41, 7516–7524. doi:10.1016/j.jeurceramsoc.2021.08.029

Tiller, F. M., and Tsai, C.-D. (1986). Theory of filtration of ceramics: I, slip casting. *J. Am. Ceram. Soc.* 69, 882–887. doi:10.1111/j.1151-2916.1986.tb07388.x

Tuersley, I. P., Jawaid, A., and Pashby, I. R. (1994). Review: various methods of machining advanced ceramic materials. *J. Mater Process Technol.* 42, 377–390. doi:10.1016/0924-0136(94)90144-9

van Noort, R. (2012). The future of dental devices is digital. *Dent. Mater.* 28, 3–12. doi:10.1016/j.dental.2011.10.014

Varanasi, V. G., Velten, M. F., Odatsu, T., Ilyas, A., Iqbal, S. M., and Aswath, P. B. (2017). "Surface modifications and surface characterization of biomaterials used in bone healing," in *Materials for bone disorders* (Netherlands: Elsevier), 405–452. doi:10.1016/B978-0-12-802792-9.00009-4

Verband der Keramischen Industrie (2022). *Breviary technical ceramics*.

Wang, F., Liu, C., Yang, H., Wang, H., Zhang, H., Zeng, X., et al. (2023a). 4D printing of ceramic structures. *Addit. Manuf.* 63, 103411. doi:10.1016/j.addma.2023.103411

Wang, H., Aboushelib, M. N., and Feilzer, A. J. (2008). Strength influencing variables on CAD/CAM zirconia frameworks. *Dent. Mater.* 24, 633–638. doi:10.1016/j.dental.2007.06.030

Wang, H., Wang, P., Wang, Q., Zhang, R., and Zhang, L. (2021). Preparation of a high-precision gama-Al2O3Structured catalyst by DLP 3D direct printing for hydrogen production from methanol. *Ind. Eng. Chem. Res.* 60, 13107–13114. doi:10.1021/acs.iecr.1c01951

Wang, K., Qiu, M., Jiao, C., Gu, J., Xie, D., Wang, C., et al. (2020a). Study on defect-free debinding green body of ceramic formed by DLP technology. *Ceram. Int.* 46, 2438–2446. doi:10.1016/j.ceramint.2019.09.237

Wang, L., Yao, L., Tang, W., and Dou, R. (2023b). Effect of Fe2O3 doping on color and mechanical properties of dental 3Y-TZP ceramics fabricated by stereolithography-based additive manufacturing. *Ceram. Int.* 49, 12105–12115. doi:10.1016/j.ceramint.2022.12.062

Wang, X., Schmidt, F., Hanaor, D., Kamm, P. H., Li, S., and Gurlo, A. (2019). Additive manufacturing of ceramics from preceramic polymers: A versatile stereolithographic approach assisted by thiol-ene click chemistry. *Addit. Manuf.* 27, 80–90. doi:10.1016/j.addma.2019.02.012

Wang, Z., Huang, C., Wang, J., Zou, B., Abbas, C. A., and Wang, X. (2020b). Design and characterization of hydroxyapatite scaffolds fabricated by stereolithography for bone tissue engineering application. *Procedia CIRP* 89, 170–175. doi:10.1016/j.procir.2020.05.138

Wei, Y., Zhao, D., Cao, Q., Wang, J., Wu, Y., Yuan, B., et al. (2020). Stereolithography-based additive manufacturing of high-performance osteoinductive calcium phosphate ceramics by a digital light-processing system. *ACS Biomater. Sci. Eng.* 6, 1787–1797. doi:10.1021/acsbiomaterials.9b01663

Wohlers, T., and Gornet, T. (2016). *History of additive manufacturing*.

Wu, H., Liu, W., He, R., Wu, Z., Jiang, Q., Song, X., et al. (2017). Fabrication of dense zirconia-toughened alumina ceramics through a stereolithography-based additive manufacturing. *Ceram. Int.* 43, 968–972. doi:10.1016/j.ceramint.2016.10.027

Wu, K. C., Seefeldt, K. F., Solomon, M. J., and Halloran, J. W. (2005). Prediction of ceramic stereolithography resin sensitivity from theory and measurement of diffusive photon transport. *J. Appl. Phys.* 98, 024902. doi:10.1063/1.1980531

Wu, Z., Liu, W., Wu, H., Huang, R., He, R., Jiang, Q., et al. (2018). Research into the mechanical properties, sintering mechanism and microstructure evolution of Al2O3-ZrO2 composites fabricated by a stereolithography-based 3D printing method. *Mater Chem. Phys.* 207, 1–10. doi:10.1016/j.matchemphys.2017.12.021

Wu, H., Chao, L., Zhang, Q., Yi, Y., Jiao, C., Ye, Y., et al. (2022). Design and 3D printing of ceramic maxillofacial prosthesis with gradient pores based on Voronoi-Tessellation principle. *Mater. Today Commun.* 33, 104559. doi:10.1016/j.mtcomm.2022.104559

Xiang, D., Xu, Y., Bai, W., and Lin, H. (2021). Dental zirconia fabricated by stereolithography: accuracy, translucency and mechanical properties in different build orientations. *Ceram. Int.* 47, 28837–28847. doi:10.1016/j.ceramint.2021.07.044

Xing, H., Zou, B., Liu, X., Wang, X., Chen, Q., Fu, X., et al. (2020a). Effect of particle size distribution on the preparation of ZTA ceramic paste applying for stereolithography 3D printing. *Powder Technol.* 359, 314–322. doi:10.1016/j.powtec.2019.09.066

Xing, H., Zou, B., Liu, X., Wang, X., Huang, C., and Hu, Y. (2020b). Fabrication strategy of complicated Al2O3-Si3N4 functionally graded materials by stereolithography 3D printing. *J. Eur. Ceram. Soc.* 40, 5797–5809. doi:10.1016/j.jeurceramsoc.2020.05.022

Xu, S., Zhang, H., Li, X., Zhang, X., Liu, H., Xiong, Y., et al. (2022). Fabrication and biological evaluation of porous β-TCP bioceramics produced using digital light processing. *Proc. Inst. Mech. Eng. H.* 236, 286–294. doi:10.1177/09544119211041186

Ye, Y., Du, Y., Hu, T., You, J., Bao, B., Wang, Y., et al. (2021). 3D printing of integrated ceramic membranes by the DLP method. *Ind. Eng. Chem. Res.* 60, 9368–9377. doi:10.1021/acs.iecr.1c02224

Yeranee, K., and Rao, Y. (2022). A review of recent investigations on flow and heat transfer enhancement in cooling channels embedded with triply periodic minimal surfaces (TPMS). *Energies (Basel)* 15, 8994. doi:10.3390/en15238994

Yin, X., Li, Q., Hong, Y., Yu, X., Yang, X., Bao, Z., et al. (2022). Customized reconstruction of alveolar cleft by high mechanically stable bioactive ceramic scaffolds fabricated by digital light processing. *Mater Des.* 218, 110659. doi:10.1016/j.matdes.2022.110659

Yuan, H., Yang, Z., Li, Y., Zhang, X., De Bruijn, J. D., and De Groot, K. (1998). Osteoinduction by calcium phosphate biomaterials. *J. Mater Sci. Mater Med.* 9, 723–726. doi:10.1023/A:1008950902047

Zakeri, S., Vastamäki, T., Honkanen, M., Järveläinen, M., Vippola, M., and Levänen, E. (2021). Fabrication of self-supporting structures made of washcoat materials (γ-Al2O3-CeO2) by ceramic stereolithography: towards digital manufacturing of enhanced catalytic converters. *Mater Des.* 210, 110115. doi:10.1016/j.matdes.2021.110115

Zakeri, S., Vippola, M., and Levänen, E. (2020). A comprehensive review of the photopolymerization of ceramic resins used in stereolithography. *Addit. Manuf.* 35, 101177. doi:10.1016/j.addma.2020.101177

Zanchetta, E., Cattaldo, M., Franchin, G., Schwentenwein, M., Homa, J., Brusatin, G., et al. (2016). Stereolithography of SiOC ceramic microcomponents. *Adv. Mater.* 28, 370–376. doi:10.1002/adma.201503470

Zhang, F., Yang, J., Zuo, Y., Li, K., Mao, Z., Jin, X., et al. (2022a). Digital light processing of β-tricalcium phosphate bioceramic scaffolds with controllable porous structures for patient specific craniomaxillofacial bone reconstruction. *Mater Des.* 216, 110558. doi:10.1016/j.matdes.2022.110558

Zhang, H., Jiao, C., He, Z., Ge, M., Tian, Z., Wang, C., et al. (2021a). Fabrication and properties of 3D printed zirconia scaffold coated with calcium silicate/hydroxyapatite. *Ceram. Int.* 47, 27032–27041. doi:10.1016/j.ceramint.2021.06.116

Zhang, J., Huang, D., Liu, S., Dong, X., Li, Y., Zhang, H., et al. (2019). Zirconia toughened hydroxyapatite biocomposite formed by a DLP 3D printing process for potential bone tissue engineering. *Mater. Sci. Eng. C* 105, 110054. doi:10.1016/j.msec.2019.110054

Zhang, K., Wei, K., Chen, J., Liang, B., Fang, D., and He, R. (2021b). Stereolithography additive manufacturing of multi-ceramic triangle structures with tunable thermal expansion. *J. Eur. Ceram. Soc.* 41, 2796–2806. doi:10.1016/j.jeurceramsoc.2020.11.033

Zhang, Y., Gao, Y., Michelin, L., Josien, L., Vidal, L., Schrodj, G., et al. (2022b). Photopolymerization of ceramic/zeolite reinforced photopolymers: towards 3D/4D printing and gas adsorption applications. *Eur. Polym. J.* 179, 111552. doi:10.1016/j.eurpolymj.2022.111552

Zhao, W., Wang, C., Xing, B., Shen, M., and Zhao, Z. (2020). Mechanical properties of zirconia octet truss structures fabricated by DLP 3D printing. *Mater Res. Express* 7, 085201. doi:10.1088/2053-1591/aba643

Zheng, T., Wang, W., Sun, J., Liu, J., and Bai, J. (2020). Development and evaluation of Al2O3–ZrO2 composite processed by digital light 3D printing. *Ceram. Int.* 46, 8682–8688. doi:10.1016/j.ceramint.2019.12.102

Zheng, W., Wu, J. M., Chen, S., Yu, K. B., Zhang, J., and Shi, Y. S. (2022). Improved mechanical properties of SiC fiber reinforced silica-based ceramic cores fabricated by stereolithography. *J. Mater Sci. Technol.* 116, 161–168. doi:10.1016/j.jmst.2021.12.012

Zhou, M., Liu, W., Wu, H., Song, X., Chen, Y., Cheng, L., et al. (2016). Preparation of a defect-free alumina cutting tool via additive manufacturing based on stereolithography – optimization of the drying and debinding processes. *Ceram. Int.* 42, 11598–11602. doi:10.1016/j.ceramint.2016.04.050

Zhou, S., Mei, H., Lu, M., and Cheng, L. (2020). 3D printed and structurally strengthened ammonia sensor. *Compos Part A Appl. Sci. Manuf.* 139, 106100. doi:10.1016/j.compositesa.2020.106100

Zhou, S., Yao, L., Mei, H., Lu, M., Cheng, L., and Zhang, L. (2022). Strengthening PPy/TiO2 arrayed SiOC honeycombs for self-protective gas sensing. *Compos B Eng.* 230, 109536. doi:10.1016/j.compositesb.2021.109536

Zhou, W. Z., Li, D., Chen, Z. W., and Chen, S. (2010). Direct fabrication of an integral ceramic mould by stereolithography. *Proc. Inst. Mech. Eng. B J. Eng. Manuf.* 224, 237–243. doi:10.1243/09544054JEM1628

Zhu, W. J., Tian, G. Q., Lu, Y., Miao, K., and Li, D. C. (2019). Leaching improvement of ceramic cores for hollow turbine blades based on additive manufacturing. *Adv. Manuf.* 7, 353–363. doi:10.1007/s40436-019-00273-2